# Chapter 4

# PROCESSING

Metal matrix composites can be made by liquid, solid, or gaseous state processes. In this chapter we describe some important processing techniques for fabricating MMCs.

## 4.1 LIQUID STATE PROCESSING

Metal matrix composites can be processed by incorporating or combining a liquid metal matrix with the reinforcement. There are several advantages to using a liquid phase route in processing. These include near net-shape (when compared to solid state processes like extrusion or diffusion bonding)), faster rate of processing, and the relatively low temperatures associated with melting most light metals, such as Al and Mg. The most common liquid phase processing techniques can be subdivided into four major categories:

- *Casting or liquid infiltration*: This involves infiltration of a fibrous or particulate preform by a liquid metal. In the case of direct introduction of short fibers or particles into a liquid mixture, consisting of liquid metal and ceramic particles or short fibers, is often stirred to obtain a homogeneous distribution of particles. In centrifugal casting, a gradient in reinforcement particle loading is obtained. This can be quite advantageous from a machining or performance perspective.

- *Squeeze casting or pressure infiltration*: This method encompasses pressure-assisted liquid infiltration of a fibrous or particulate preform. This process is particularly suited for complex shaped components, selective or localized reinforcement, and where production speed is critical.

- *Spray co-deposition*: In this process the liquid metal is atomized or sprayed while a particle injector introduces ceramic particles in the

spray stream to produce a granulated mixture of composite particles. The composite particles are then consolidated using another suitable technique, such as hot-pressing, extrusion, forging, etc.

- *In situ processes*: In this case, the reinforcement phase is formed *in situ* either by reaction during synthesis or by controlled solidification of a eutectic alloy.

We now discuss each of these processing classes in detail.

### 4.1.1 Casting

*Conventional Casting*

Casting of MMCs can typically be accomplished with conventional equipment used to cast metallic alloys (Surappa and Rohatgi, 1981). It is typically used with particulate reinforcement because of the difficulty in casting fibrous performs without pressure. The particles and matrix mixture are cast into ingots and a secondary mechanical process, such as extrusion or rolling, is applied to the composite, see Fig. 4.1.

Casting of MMCs requires some modifications to existing conventional casting processes, which can be summarized as follows:

- Alloys that minimize reactivity with the reinforcement must be used. Al-Si alloys (with Si levels of up to 9%) are typically used with SiC reinforcement. Figure 4.2 shows that with increasing temperature, an increase in the amount of silicon is required to prevent $Al_4C_3$ formation

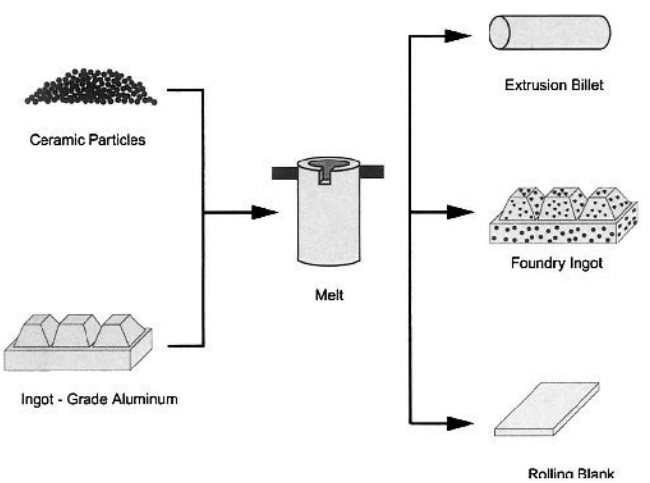


**Fig. 4.1** Conventional casting route for processing particle reinforced MMCs.

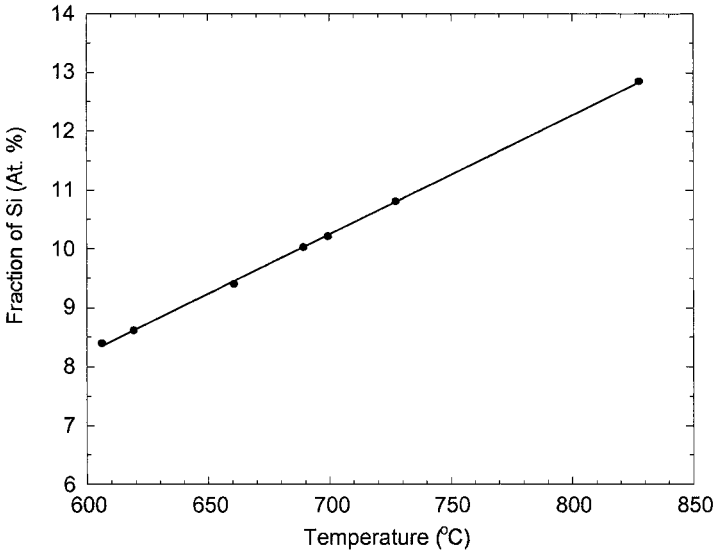


**Fig. 4.2** Fraction of Si, at a given temperature, required to prevent formation of $Al_4C_3$ in an Al-Si/SiC composite (after Lloyd, 1997).

(see chapter 5).

- Addition of reinforcement particles increases the viscosity of the melt. For a viscous non-metallic liquid with nonmetallic particles, the viscosity of the composite, $\eta_c$, is given by (Thomas, 1965):

$$\eta_c = \eta_m\left(1 + 2.5V_p + 10.05V_p\right)$$

where $\eta_m$ is the viscosity of the unreinforced metal and $V_p$ is the volume fraction of particles. Thus, the temperature of the composite melt should be above a certain limit (~745°C for Al-Si/SiC) to keep the melt from becoming too viscous. Covering the melt with an inert gas atmosphere reduces oxidation of the melt.

- Stirring of the composite melt is often required, Fig. 4.3 (Mehrabian et al., 1974). The density of SiC (3.2 g/cm$^3$), for example, is higher than that of Al (2.2 g/cm$^3$), so the particles will sink unless the melt is agitated. Alternating currents in a magnetic field (Katsura, 1982) and mechanical vibration (Pennander and Anderson, 1991) have also been used to improve wetting and permeability of the reinforcement in the liquid matrix.

*Centrifugal Casting*

One of the disadvantages of MMCs with ceramic reinforcement is that they are typically more difficult to machine than the unreinforced alloy. In centrifugal casting, optimal placement of the reinforcement can be achieved by inducing a centrifugal force immediately during casting, Fig. 4.4, to intentionally obtain a gradient in reinforcement volume fraction (Divecha et al., 1981; Tsunekawa et al., 1988). In brake rotors, for example, wear resistance is needed on the rotor face, but not in the hub area. Thus, in areas where reinforcement is not as crucial, such as in the hub area, machining would be easier without the reinforcement. Figure 4.5 shows the microstructure at different points in a centrifugally-cast brake rotor, showing

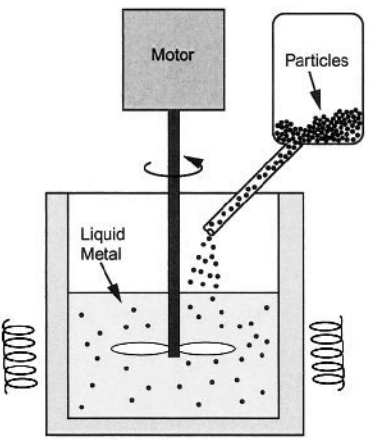


**Fig. 4.3** Stirring of composite melt with ceramic particles to minimize settling of the particles during processing.

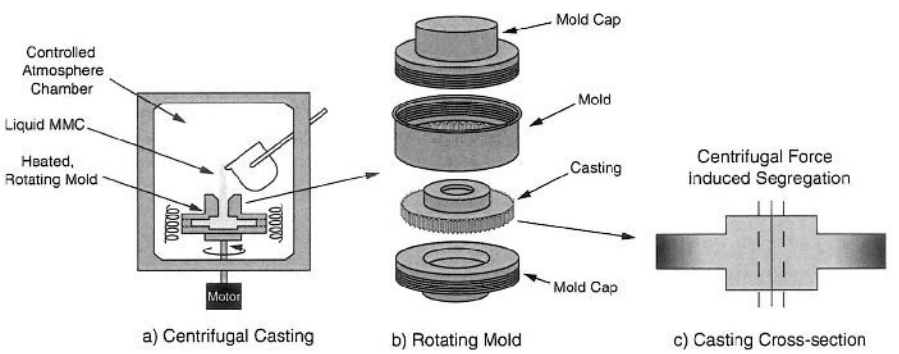


**Fig. 4.4** (a) Schematic of centrifugal casting process, (b) rotating mold, and (c) cross-section of finished casting with intentionally-segregated reinforcement.

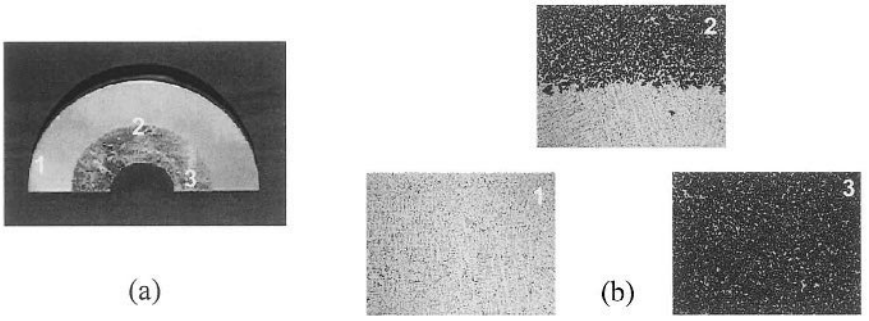


**Fig. 4.5** (a) Centrifugally cast brake rotor with selective placement of reinforcement, and (b) regions of the microstructure in the rotor: (1) matrix-rich, (2) interface, (3) reinforcement-rich (courtesy of D. Herling).

a pure aluminum alloy matrix region, interface region, and reinforced region. The process is relatively inexpensive, with a potential for composite materials at as low as $ 2/kg.

*Microstructure Evolution during Casting*

During casting the reinforcement (particle or short fiber) is typically mobile, so that motion or pushing of the particle by the liquid needs to be considered. If the particles are pushed by the solidifying liquid, the particles are segregated to the remaining liquid that solidifies. In eutectic systems, for example, the remaining liquid is highly rich in solute. The resulting microstructure, then, depends on the relative size of the primary dendrites relative to the particle size. For composites cooled at relatively slow cooling rates, the dendrite size is much larger than the particle size and the solidified microstructure consists of several areas of high particle clustering, Fig. 4.6 (Lloyd, 1994). For faster cooling rates, the matrix cell size is much smaller (on the order of the particle size) so the degree of particle pushing is diminished significantly, resulting in a much more homogeneous distribution of particles, Fig. 4.7.

Experimental studies on particle pushing in particle reinforced MMCs show the following trends: (i) in eutectic and hypereutectic matrix alloys, such as Al-Si, particle capture takes place for all growth conditions, (ii) in hypoeutectic Al alloy systems, where a non-planar solid/liquid interface is typically present, particle pushing takes place, and (iii) in several systems, there is a critical velocity of the solid/liquid interface, $V_c$, below which particle pushing takes place and above which particle capture occurs. For a planar solid/liquid interface, $V_c$ can be related to the particle diameter, d, by the following relationship (Mortensen and Jin, 1992):

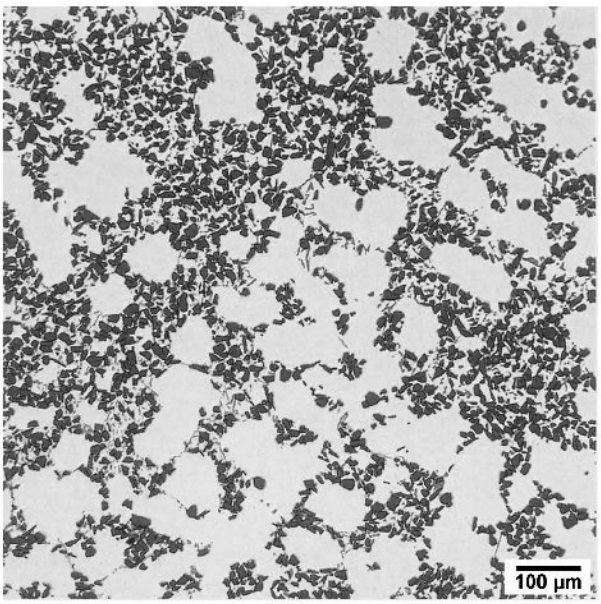


(a)

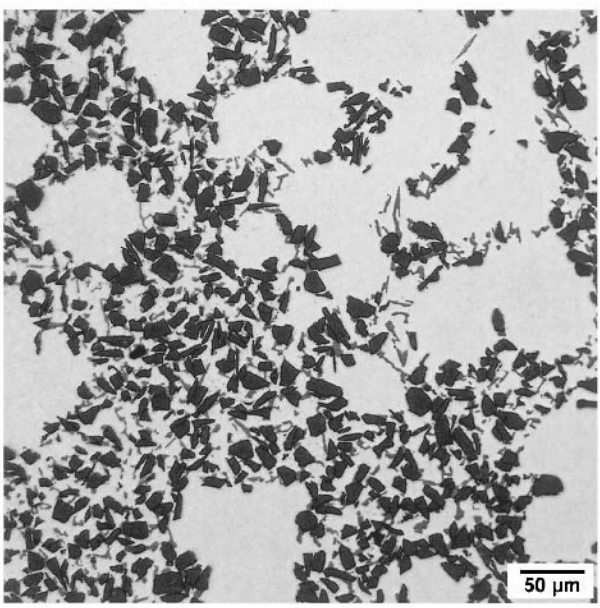


(b)

**Fig. 4.6** Highly clustered SiC particle distribution in Al resulting from slow cooling, due to particle pushing: (a) lower magnification and (b) higher magnification (courtesy of D.J. Lloyd).

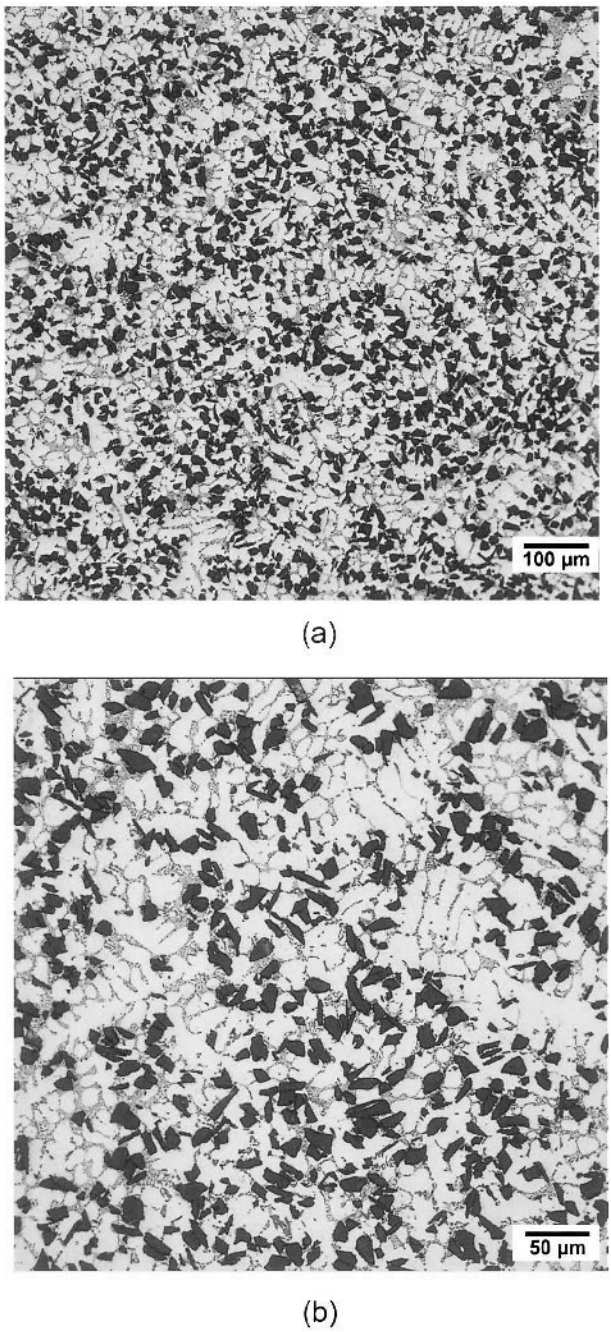


**Fig. 4.7** Uniform SiC particle distribution in Al resulting from faster cooling: (a) lower magnification and (b) higher magnification (courtesy of D.J. Lloyd).

$$V_c d^n = C$$

where C is a system-dependent constant and the exponent n varies between 0.5-3.

Two criteria have generally been proposed for particle pushing. The first is related to the free energy change as the solid grows and comes into contact with the particle in the liquid. Uhlmann et al. (1964) and Potschke and Rogge (1989) proposed the following criterion for particle pushing, based on interfacial free energies:

$$\gamma_{ps} > \gamma_{pl} + \gamma_{sl}$$

where $\gamma$ is the interfacial energy, and the subscripts ps, pl, and sl refer to particle/solid, particle/liquid, and solid/liquid interfaces, respectively. This model is generally only valid when the interface velocities are small and it is not of great practical interest because the interfacial free energies are largely unknown.

Several investigators have taken a different, more practical approach, of trying to predict the critical interface velocity for particle pushing (Uhlmann et al., 1964; Cisse and Bolling, 1971; Stefanescu et al., 1988; Shangguan et al., 1992; and Kim and Rohatgi, 1999). This approach is based on experimental observations that a critical interface velocity exists, below which the particles are pushed, and above which the particles are engulfed. Cisse and Bolling (1971) modeled the balance between the viscous drag on the particle and the counteracting repulsing force exerted by the particle on the solid/liquid interface front, and proposed a critical velocity for particle pushing/engulfment:

$$V_c^2 = \frac{4kT\gamma_{sl}a_o}{9\pi\eta^2 R^3}\frac{\alpha(1-\alpha)^3}{(1-3\alpha)}$$

where $\eta$ is the viscosity of the liquid, T is temperature, $\gamma$ is the free energy of the solid/liquid interface, R is the radius of the particle, $a_o$ is the distance between the particle and the solid/liquid interface, k is the curvature of the solid/liquid interface, and $\alpha$ is the ratio of particle radius to interface radius. Kim and Rohatgi (1999) modeled the shape of the solid/liquid front in terms of the ratio of thermal conductivity of the particle to that of the liquid, the

temperature gradient and surface tension of the solid/liquid interface, and the heat of fusion of the liquid. They derived the following expression:

$$V_c = \frac{\Delta\gamma a_o (kR + 1)}{18\eta R}$$

where $\Delta\gamma$ is the difference in interface energy, $\Delta\gamma = \gamma_{sp} - \gamma_{lp} - \gamma_{sl}$. Kim and Rohatgi (1999) showed that their model was closest to experimental measurements of the critical velocity, compared to other models, yet, their prediction was still a factor of 2 lower than that of the experimental values. This was attributed to the fact that (a) a constant particle temperature was used in the calculations, when in reality, the particle temperature may be changing with time, and (b) factors such as particle shape, particle roughness, and heat convection between the particle and the interface, were not considered in the model.

### 4.1.2 Liquid Infiltration

*Liquid Infiltration (Lanxide™ Process)*

Another pressureless infiltration process consists of reactive or non-reactive infiltration of a reinforcement preform. In this process a particulate or fribrous filler is infiltrated with pure Al or Al-Mg alloy, Fig. 4.8. Alloy matrices may also be formed in this process. For example, when pure Al is

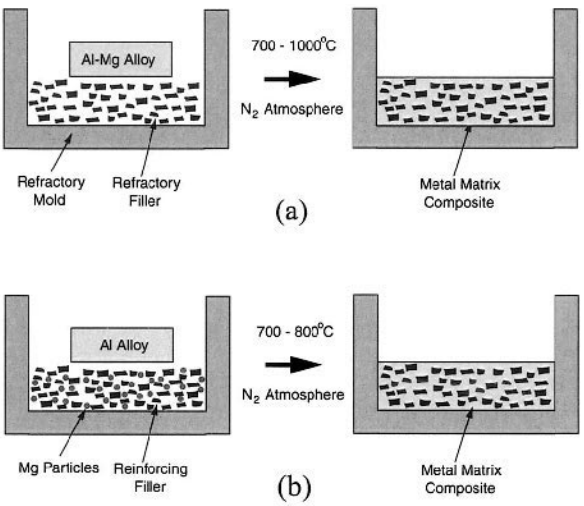


**Fig. 4.8** Pressureless infiltration of MMCs: (a) Alloy matrix infiltration of particulate preform and (b) pure matrix infiltration of metallic alloy particle and ceramic particulate preform.

intermingled with Mg particles (in addition to the ceramic reinforcement particles) an Al-Mg alloy matrix is formed. The process is conducted in $N_2$ atmosphere to minimize interfacial reactions, particularly since the pressureless process involves long infiltration times at high temperatures (Aghajanian et al., 1989). When pure Al is infiltrated, the infiltration temperatures are between 700-800°C, while infiltration of Al-Mg alloys is conducted between 700-1000°C (Lloyd, 1997). Typical infiltration rates are less than 25 cm/h.

*Squeeze Casting*

Squeeze casting or pressure infiltration involves forcing the liquid metal matrix into a short fiber or particulate preform (Mortensen et al., 1988; Masur et al., 1989; Cook and Werner, 1991). The main advantages of this method over conventional casting are the shorter processing times (which is of particular interest for production of materials in high volumes), ability to fabricate relatively complex shapes, minimal residual porosity or shrinkage cavities due to the applied pressure, and minimization of interfacial reaction products between reinforcement and matrix (due to the shorter processing times). Before infiltration takes place, the reinforcement preform must be prepared. Figure 4.9 shows two processes for making the preform: (a) press forming and (b) suction forming. In the press forming process, an aqueous slurry of fibers is agitated and poured into a mold, pressure is applied to squeeze out the water, and the preform is dried. In the other process, suction

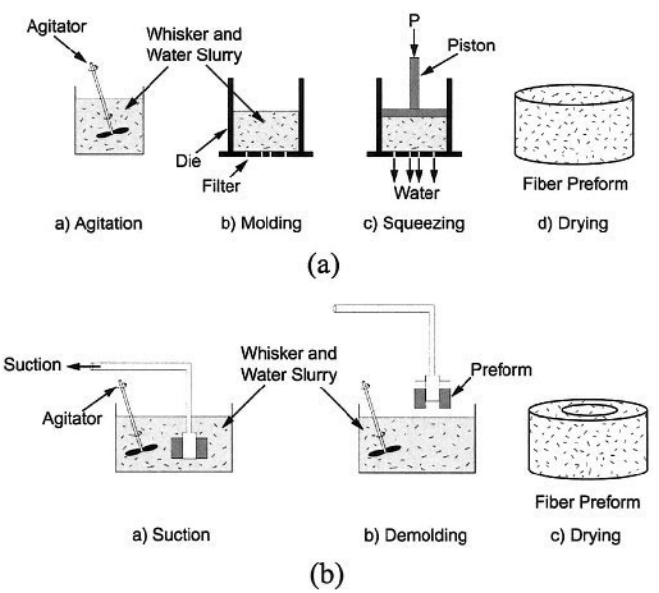


**Fig. 4.9** Processes for making particulate performs: (a) press forming and (b) suction forming.

is applied to the mixture that consists of the reinforcement, fiber, and water. The mixture is then demolded and dried.

In order to obtain infiltration of the preform, the molten metal must have a relatively low viscosity and good wettability of the reinforcement. A schematic of the liquid infiltration process is shown in Figure 4.10. The reinforcement preform is placed in a mold, and the liquid is poured into a preheated die located on the bed of a hydraulic press. Infiltration takes place by mechanical force or by using a pressurized inert gas. Applied pressures on the order of 70-100 MPa are typically used. Having the preform temperature lower than that of the matrix liquidus temperature is highly desirable in order to minimize interfacial reaction and to obtain a fine matrix grain size.

Squeeze casting can also be used to obtain composites with relatively high reinforcement volume fractions (> 40%) (Mortensen et al., 1988; Saha et al., 2002). In conventional casting, achieving homogeneous particle packing and distribution at high volume fractions of reinforcement is problematic. Figure 4.11 shows the microstructure of a 6060 Al matrix composite reinforced with 50% SiC particles. Note the fine interparticle spacing and absence of any residual porosity. This technique has also been used to fabricate continuous fiber reinforced MMCs (Deve´ and McCullough, 1995). Figure 4.12 shows a microstructure of $Al_2O_3$ fibers (Nextel 610) in a pure Al matrix infiltrated by 3M. The distribution of fibers is relatively uniform, although some "channels" of pure matrix were formed during infiltration.

Although the squeeze casting technique has been primarily used for infiltrating low melting point metals, such as Al, continuous fiber reinforced intermetallic matrix composites such as $Al_2O_3$ reinforced TiAl, $Ni_3Al$, and $Fe_3Al$ have also been processed (Nourbakhsh et al., 1990). The process is similar to that for discontinuously reinforced MMCs. A mixture of the matrix alloy with wetting-enhancing additives is melted in a crucible, while

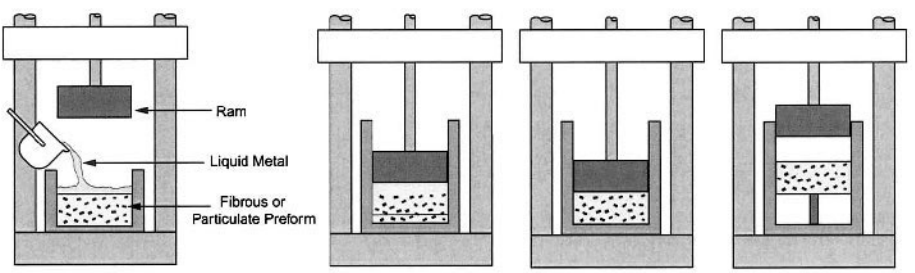


**Fig. 4.10** Schematic of squeeze casting process.

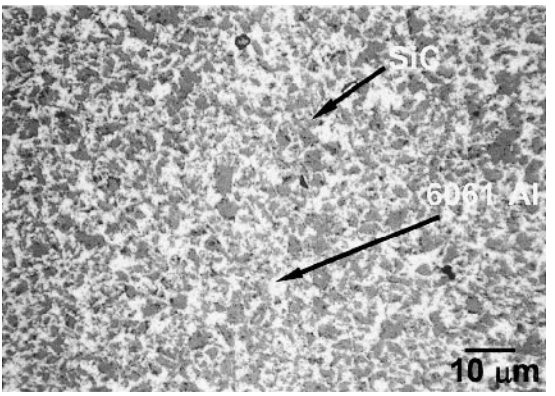


**Fig. 4.11** Microstructure of 6061/SiC/$50_p$ composite. Notice the large volume fraction of particles and relatively small interparticle spacing (Saha et al., 2000).

the fibrous preform is heated separately. The molten metal is then poured onto the fibers, and pressure is applied simultaneously, via argon gas, to infiltrate the preform.

*Infiltration Mechanics*

Infiltration of the liquid matrix through a particulate or fibrous preform can be thought of as liquid infiltration of a porous medium. As such, the capillarity of the liquid and its permeability in the preform will affect the infiltration characteristics of the metal through the porous reinforcement. The reader is referred to an excellent review by Michaud (1993) for details. Here we provide some salient points on the mechanics of infiltration in MMCs. Consider infiltration of a liquid phase with velocity $v_L$ through a small volume $\Delta V$, Fig. 4.13 (Michaud, 1993). The volume consists of fiber, matrix, and porosity, so the sum of the volume fractions, $V_f$, $V_m$, and $V_p$, is equal to 1. The velocity of the solid preform, $v_s$, is also taken into consideration, although we can neglect deformation of the preform during infiltration, so $v_s = 0$. A fraction of the liquid metal, $g_s$, will gradually solidify during infiltration so the volume fraction of solid matter in the composite (fibers plus solidified metal) is given by $V_{sf} = V_f + g_s V_m$.

We can now discuss the liquid infiltration processes, in terms of the parameters described above, using the Forscheimer equation, used to describe flow in a porous medium:

$$f - \nabla P = \left[ \frac{\eta V_m (1 - g_s)}{K} + B\rho_m \sqrt{(v_l - v_s)^2} \right] (v_l - v_s)$$

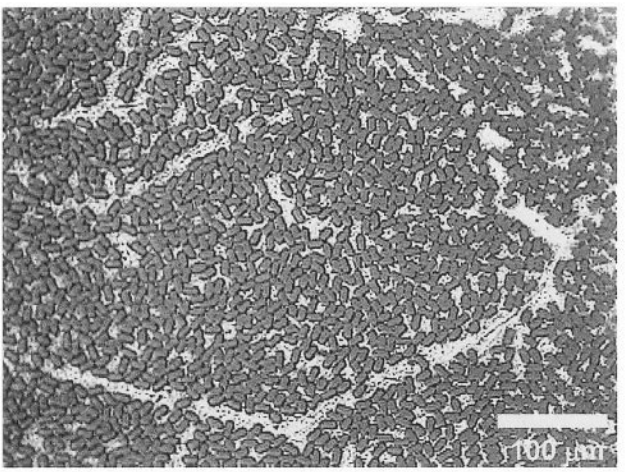


(a)

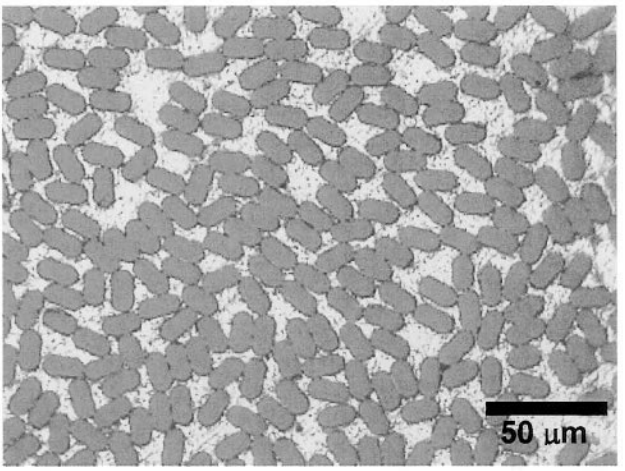


(b)

**Fig. 4.12** Microstructure of liquid infiltrated $Al_2O_3$ fiber (Nextel 610) reinforced pure Al matrix composite. (a) low magnification and (b) high magnification. The distribution of fibers is relatively uniform, although some "channels" of pure matrix were formed during infiltration (indicated by arrows).

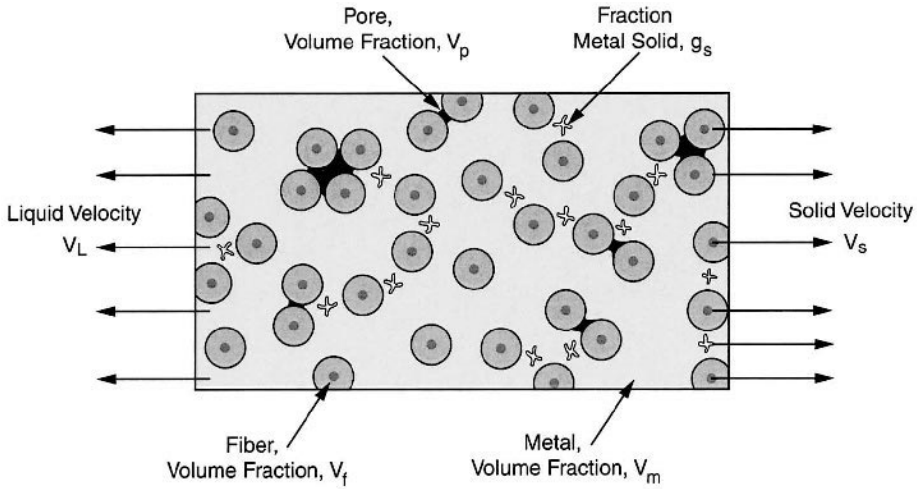


**Fig. 4.13** Schematic of parameters associated with liquid infiltration of a metal matrix through a porous reinforcement preform (after Michaud, 1993).

where f is the volumetric gravitational, centrifugal, or electromagnetic force, P is the average pressure applied in the volume $\Delta V$, $\eta$ is the viscosity of the liquid metal, $\rho_m$ is the density of the liquid metal, and $v_l$ and $v_s$ are the velocity of the liquid and solid, respectively. K is termed the permeability of the preform and B is a constant. K is a function of the reinforcement preform microstructure, wetting characteristics, reactivity, etc., as well as $V_m$, the matrix volume fraction, and characteristics of the solidified metal. The relevant Reynolds number for a preform with characteristic length d (for example, fiber diameter), is given by:

$$R_e = \frac{d\rho_m \sqrt{(v_l - v_s)^2}}{\eta V_f}$$

where $V_f$ is the fiber volume fraction and the other symbols have the significance given earlier. When $R_e$ is below a critical value of the Reynolds number, $R_{e,critical}$, (approximately equal to 1 for the preform considered here), the second term in the Forscheimer equation can be neglected, and we obtain Darcy's law:

$$v_l - v_s = \frac{K}{\eta V_m (1 - g_s)} (f - \nabla P)$$

The left-hand side of the equation can be thought of as a volumetric density of the fluid (i.e., $\frac{\text{volume}}{\text{area} \cdot \text{time}}$). It can be recognized that Darcy's law is an

analog of Ohm's law for electrical conduction, i.e., permeability is analogous to electrical conductivity. Thus, in general, higher permeability, lower viscosity, and higher applied pressure will contribute to faster infiltration of the liquid matrix into the reinforcement preform.

Analysis of heat transfer during the matrix infiltration process is important because as the liquid metal infiltrates and solidifies it will release heat into its surroundings. The heat flow will cause an increase in temperature of the system, allowing incoming liquid to remain in the liquid state while infiltrating the preform. In practice, liquid flow ceases when enough cooling from the preform and/or partially solidified composite takes place, or when the preform is completely filled. In general, heat transfer within the volume element $\Delta V$ is dictated by conduction, convention, exothermic characteristics of interfacial reactions, and the fraction of total solidified metal, $g_s$. The governing equation for this heat transfer is (Michaud, 1993):

$$\nabla \cdot (k_c \nabla T) = \rho_c c_c \frac{\partial T}{\partial t} + \rho_m c_m V_m (1 - g_s) v_l \cdot \nabla T$$
$$+ (\rho_f c_f V_f + \rho_m c_m V_m g_s) v_s \cdot \nabla T - \rho_m \Delta H \frac{\partial (g_s V_m)}{\partial t} - \dot{Q}$$

where $k_c$ is the thermal conductivity of the composite, $\Delta H$ is the latent heat of solidification of the metal, and $\dot{Q}$ is the rate of heat released from any chemical reaction. $\rho$ and c refer to the density and heat capacity, respectively, and the subscripts f, m, and, c denote the reinforcement, metal, and composite, respectively.

Mass transfer also needs to be considered when analyzing the liquid infiltration process. Because of the relatively short time scales involved with most infiltration processes, the contribution from diffusion to mass flow within $\Delta V$ can be neglected. Rather, convection plays a more prominent role, due to solution or rejection of a solute in the metal (for an alloy) and consumption during an interfacial chemical reaction. The governing relation for mass transport is:

$$\frac{\partial \overline{C}}{\partial t} = -\nabla \cdot [(1 - g_s) C_l v_l + g_s C_s v_s] + r_A$$

where $\overline{C}$ is the average matrix composition, $r_A$ is the rate of change in solute due to the chemical reaction, and $C_l$ and $C_s$ are the composition of the liquid

and solid phases, respectively, as determined from the phase diagram of the alloy at a given temperature.

*Microstructure Evolution during Liquid Phase Infiltration*

The microstructure of the composite during infiltration depends on the local solidification and cooling processes within the preform. The liquid metal will solidify when it comes in contact with the preform, which is at a lower temperature. A schematic of the infiltration front, temperature distribution in the preform, and grain size distribution in the matrix is shown in Figure 4.14 (Mortensen and Jin, 1992). At the infiltration front, the metal will solidify first (Region 1), while in the middle of the preform (Region 2), a relatively constant temperature is obtained. The semi-solid metal close to the infiltration gate (Region 3), however, will continuously be in contact with the liquid metal. The situation is more complicated for a binary eutectic alloy. The infiltration front, temperature distribution and liquid metal composition, for a binary alloy matrix composite, are shown in Figure 4.14(b). The temperature gradient is similar to that of the pure metal, but a significant amount of solute segregation takes place at the infiltration front. Thus, the remaining incoming liquid is depleted of solute.

Grain size distribution will also be affected by the local temperature distribution and cooling rate. For infiltration of the pure alloy, Figure 4.14(b), in Region 1 a fine matrix grain size is obtained because the molten metal comes into contact with the cooler reinforcement preform, which results in rapid solidification of the matrix. Heterogeneous nucleation at the reinforcement does not occur in most MMCs processed by liquid phase (Mortensen and Jin, 1992). In most Al matrix composites, for example, the grain size is usually much larger than the reinforcement size. The exception to this is in Al-Si matrix composites, where the primary Si phases nucleates preferentially at the reinforcement. Thus, in these composites, the composite has a finer distribution of Si phase, compared to the unreinforced alloy. Figure 4.15 shows the cell size in 6061 matrix composites, reinforced with 10 and 20% SiC particles (Lloyd, 1989). Note that the composite has a finer overall microstructure than the unreinforced alloy, at all cooling rates.

In some cases, particularly where fiber reinforcement is involved, the reinforcement actually impedes heat convection from the liquid metal, resulting in a larger degree of columnar dendritic growth than in the unreinforced alloy (Cole and Bolling, 1965). In Region 2, the grain size is slightly larger because of the higher temperatures and somewhat lower cooling rate. Finally, at the gate a coarser microstructure will result, as this

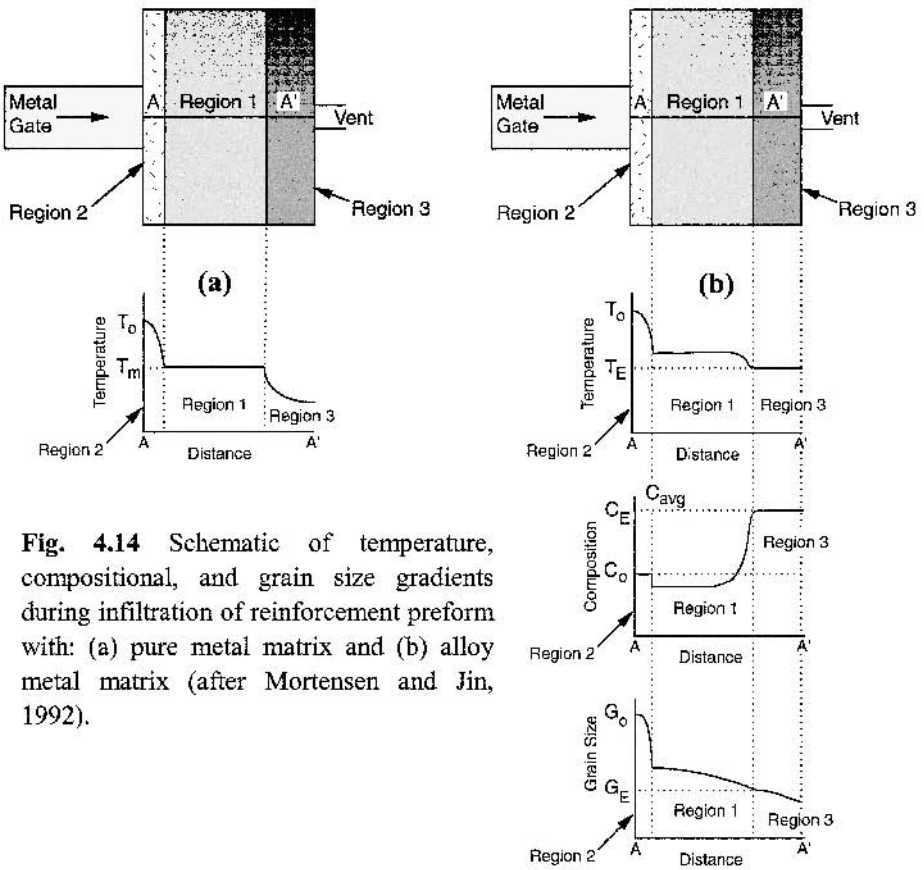


**Fig. 4.14** Schematic of temperature, compositional, and grain size gradients during infiltration of reinforcement preform with: (a) pure metal matrix and (b) alloy metal matrix (after Mortensen and Jin, 1992).

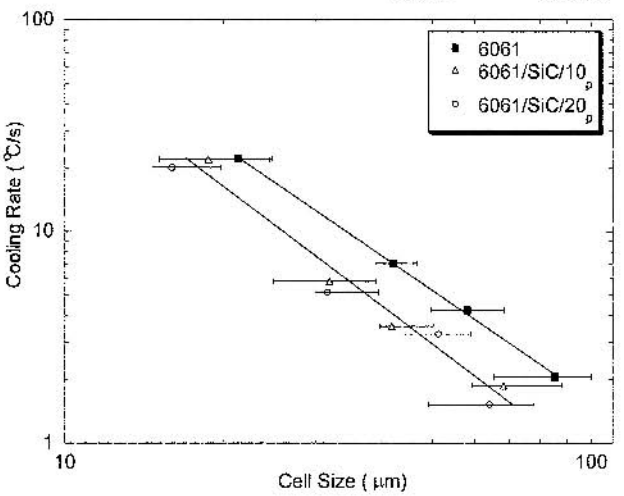


**Fig. 4.15** Cooling rate vs. matrix cell size in Al 6061 matrix composites, reinforced with 10 and 20% SiC particles (Lloyd, 1989). Note that the composite has a finer overall microstructure than the unreinforced alloy, at all cooling rates, because of pinning of the reinforcement particles.

region will be the last to solidify and will cool at a relatively slow rate. Figure 4.16 shows the microstructure of a Saffil ($Al_2O_3$) fiber reinforced Al-4.5Cu matrix, where the matrix microstructure well within the preform is much finer than that close to the infiltration gate.

The microstructure of the matrix is not only a function of the temperature and composition gradients, but also on the velocity of the liquid and the interfiber spacing. Shekhar and Trivedi (1989, 1990) studied the solidification processes in model fiber and particle-containing organic transparent systems. In fiber reinforced systems, as the interfiber spacing approaches the primary dendrite or cell spacing, perturbations in the advancing liquid cause morphological changes upon solidification. The effect of velocity and interfiber spacing (indicated by the ratio of interfiber spacing, d, to the primary dendrite spacing $\lambda$) can be represented by a

microstructure map, Figure 4.17 (Trivedi et al., 1990). For very large interfiber spacing, the morphology is dependent on the liquid velocity, going from planar to cellular to dendritic with increasing velocity. When the interfiber spacing is very small, the cellular regime is larger since both planar and dendritic structures will transform to cellular structures. At intermediate spacing, dendritic microstructures will be observed at lower velocities, when the ratio of $d/\lambda$ is slightly greater than 1.

### 4.1.3 Spray Co-deposition

Spray deposition has been used for some time to fabricate metallic alloys in powder form (Lavernia et al., 1992). The metal or alloy is melted and the liquid stream is atomized with water or an inert gas. Rapid solidification of the liquid takes place, resulting in a fine solid powder. This technique has been modified, by injecting reinforcement particles or co-depositing the particles with the matrix alloy, Figure 4.18, (Lloyd, 1997). The advantage of this technique is the high rate of production, which can approach 6-10 kg/min, and the very fast solidification rate, which minimizes any reaction between particle and matrix. The as-processed billet is not fully dense, so secondary processing is required to fully densify and homogenize the composite. The distribution of particles in the liquid droplet is very much dependent on the size of the reinforcement and at what point in the process the reinforcement is injected into the matrix (Lloyd, 1997). Whiskers, for example, are too fine to be optimally injected and distributed in the liquid droplets. When the particles are injected into the matrix immediately after atomization, the matrix is still liquid, so the particles are able to envelope themselves into the liquid droplet, and a relatively homogenous distribution

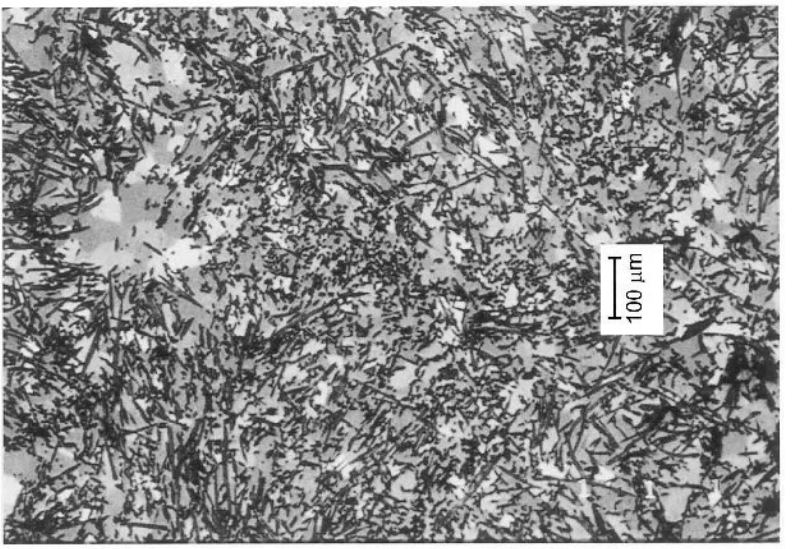


(a)

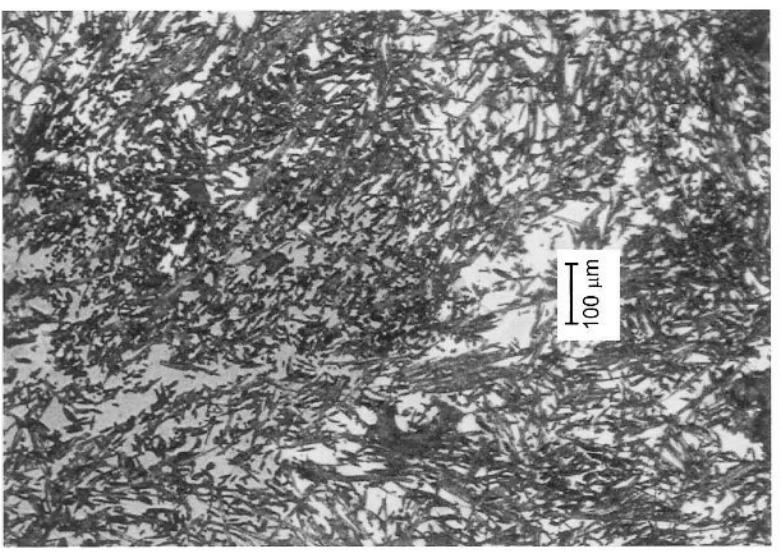


(b)

**Fig. 4.16** Microstructure of a Saffil ($Al_2O_3$) fiber reinforced Al-4.5Cu matrix. The matrix grain size well within the preform (a), is much finer than that close to the infiltration gate (b), since the latter goes through remelting and much slower cooling (courtesy of V. Michaud).

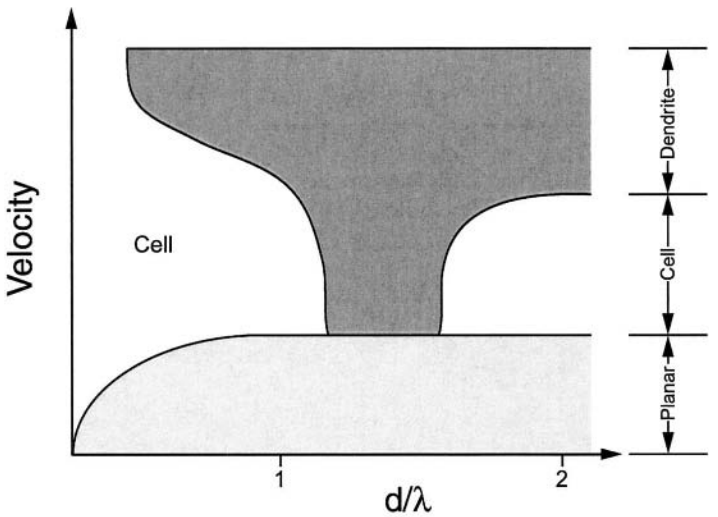


**Fig. 4.17** Effect of solidification front velocity and interfiber spacing (represented by the ratio of interfiber spacing, d, to dendrite spacing, λ) on matrix microstructure. For very large d/λ, the morphology goes from planar to cellular to dendritic with increasing velocity. When the interfiber spacing is very small, the cellular regime is larger since both planar and dendritic structures will transform to cellular structures (after Trivedi et al., 1990).

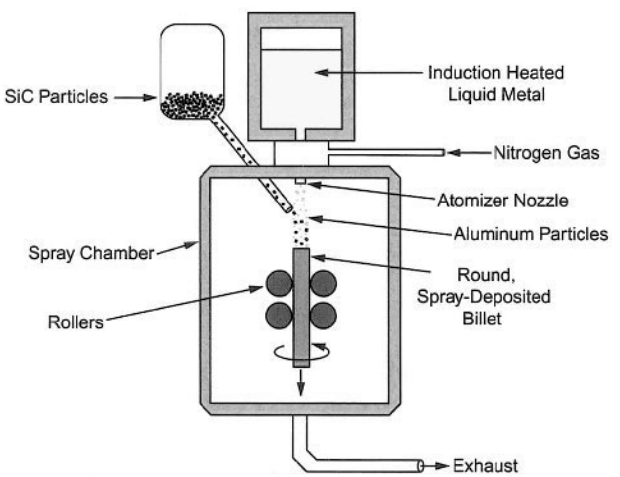


**Fig. 4.18** Spray co-deposition of SiC particles and Al liquid droplets, to form composite particles.

of particles in the matrix is obtained, Figure 4.19(a). Injection of the particles later in the process, i.e., when the matrix droplet is semisolid, does not allow

easy ingression of the particles into the matrix, causing the particles to reside along the periphery of the matrix particle, Figure 4.19(b). A consolidated composite with the latter particle size distribution will have inferior properties as a result of a high degree of particle clustering. This process is quite flexible in that the metal and reinforcement sprayers can be tailored to obtain in situ laminates or even functionally graded materials. The process can be quite expensive, however, owing to the high cost of the capital equipment.

### 4.1.4 *In Situ* Processes

*In situ* processes fall into two major categories: Reactive and non-reactive processes. In the reactive processes two components are allowed to react exothermically to form the reinforcement phase. The XD process is an example of this process (Martin Marietta, 1987). Typically, a rather high volume fraction of ceramic particles is formed in the matrix alloy, and this master alloy is diluted with the matrix alloy to obtain a composite of desired reinforcement volume fraction. Typical examples involve TiB and TiC as reinforcement particles, which are formed by the following reactions:

$$2B + Ti + Al \rightarrow TiB_2 + Al$$

and

$$C + Ti + Al \rightarrow TiC + Al$$

Processing variables such as reaction temperature can be used to tailor the desired reinforcement particle size, which is usually in the 0.25-1.5 μm

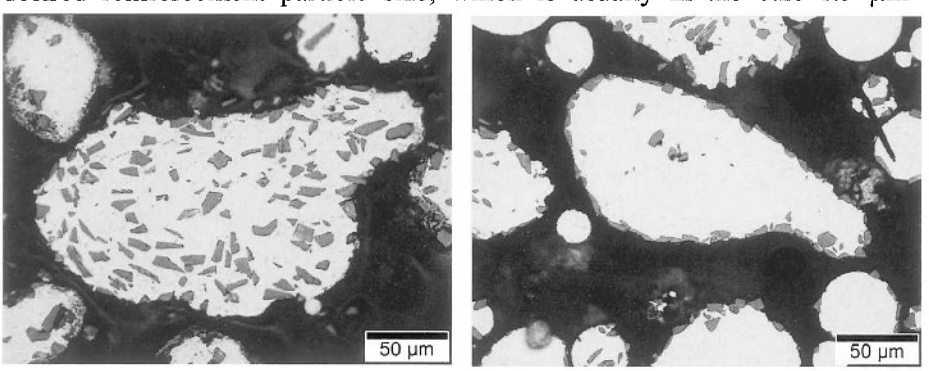


**Fig. 4.19** Microstructure of composite particles obtained from spray co-deposition: (a) homogeneous particle distribution for particle injection while matrix is in liquid state and (b) particles at periphery of matrix droplet, due to particle injection when the matrix is in a semi-solid state (courtesy of D. Lloyd).

range. The matrix commonly is Al, Ni, or an intermetallic matrix. An alternative process that combines spray co-deposition and reaction is to atomize an Al-Ti alloy (at sufficiently high temperature) with a C-containing gas to form TiC particles (Chawla, 1997). The advantage of *in situ* reaction processes, in general, is that the reaction eliminates problems typically associated with wetting of the particle, so a relatively clean and strong interface is typically formed (Christodolou et al., 1988). The number of composite systems where reaction processing is beneficial, however, is limited, and the relatively fine size distribution of particles produced can significantly increase the viscosity of the melt.

Non-reactive *in situ* processes take advantage of two-phase systems, such as eutectic or monotectic alloys, to form the fiber and matrix in situ (McLean, 1983). Controlled directional solidification is conducted to separate the two phases, as shown in Fig. 4.20. A precast and homogenized material is melted in a graphite crucible, and contained in a quartz tube in vacuum or inert gas atmosphere. Heating is typically conducted by induction and the thermal gradient is obtained by chilling the crucible. Electron beam heating may also be used, particular when using reactive metals such as titanium. One can control the fineness of the microstructure, i.e., the size and spacing of the reinforcement (at constant volume fraction) by controlling the solidification rate. These rates typically lie in the range of 1-5 cm/h due to the need to maintain a stable solidification growth front. Figure 4.21 shows a cross-section of the microstructure of an *in situ*-processed composite.

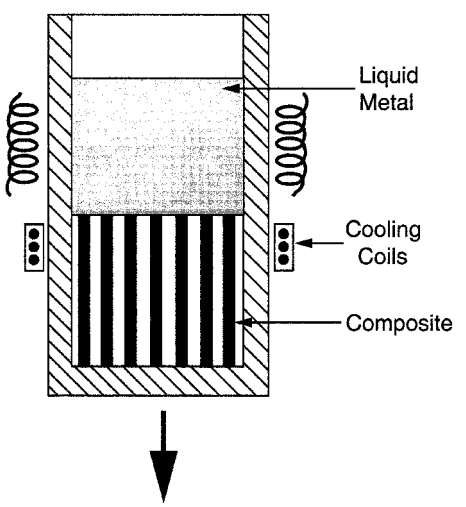


**Fig. 4.20** Schematic of directional solidification process to obtain *in situ* composites.

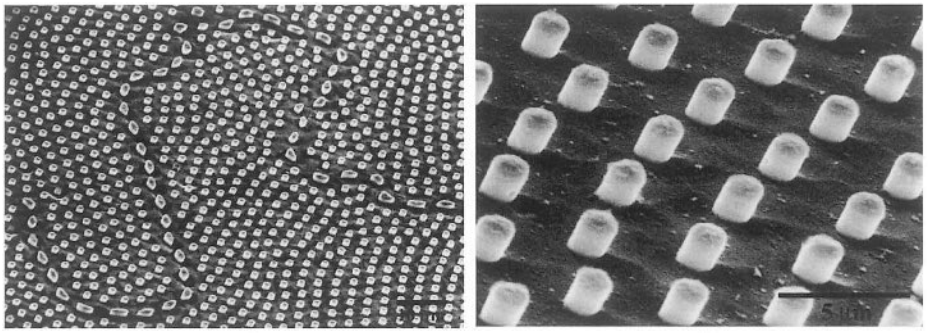


**Fig. 4.21** Cross-section of the microstructure of an *in situ* processed composite: (a) lower magnification and (b) higher magnification. The matrix has been etched out locally to show the fibers. Note that the fibers at grain boundaries are somewhat coarser due to earlier nucleation and growth, relative to the fibers within the grain (courtesy of J.B. Andrews).

## 4.2 SOLID STATE PROCESSING

The main drawback associated with liquid phase techniques is the difficulty in controlling reinforcement distribution and obtaining a uniform matrix microstructure (Michaud, 1993). Furthermore, adverse interfacial reactions between the matrix and the reinforcement are likely to occur at the high temperatures involved in liquid processing. These reactions can have an adverse effect on the mechanical properties of the composite (Sahoo and Koczak, 1991; Chawla, 1997). The most common solid phase processes are based on powder metallurgy techniques (Ghosh, 1993). These typically involve discontinuous reinforcements, due to the ease of mixing and blending, and the effectiveness of densification. The ceramic and metal powders are mixed, isostatically cold compacted, and hot-pressed to full density. The fully-dense compact then typically undergoes a secondary operation such as extrusion or forging (Lloyd, 1997). Novel low-cost approaches, such as sinter-forging, have aimed at eliminating the hot pressing step, with promising results (Chawla et al., 2003).

### 4.2.1 Powder Metallurgy Processing

Powder processing involves cold pressing and sintering, or hot pressing to fabricate primarily particle- or whisker-reinforced MMCs (Hunt, 1994). The matrix and the reinforcement powders are blended to produce a homogeneous distribution. Figure 4.22 shows a blended powder mixture of Al, 50Al-50Cu (wt.%), and SiC particles. The 50Al-50Cu articles are added to provide a uniform distribution of the alloying additions, while the pure Al

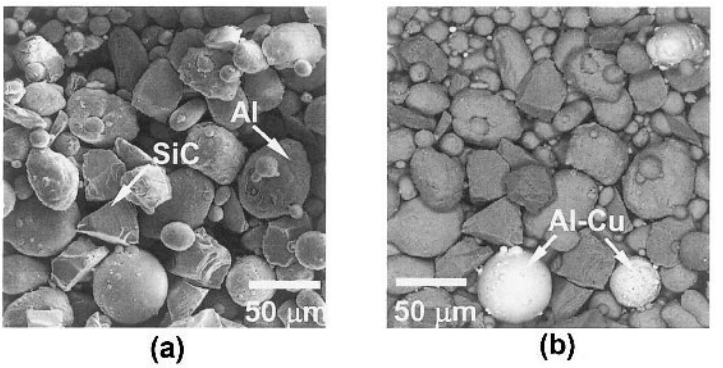


**Fig. 4.22** Powder mixture of Al, SiC, and 50wt.%Al-50wt.%Cu particles (Chawla et al., 2003): (a) secondary electron image, and (b) backscattered electron image, showing the Al-Cu particles.

particles enable easier cold pressing. The blending stage is followed by cold pressing to produce what is called a green body, which is about 80% dense and can be easily handled, Fig. 4.23. The cold pressed green body is canned in a container, sealed, and degassed to remove any absorbed moisture from the particle surfaces. One of the problems with bonding metallic powder particles, such as Al particles, to ceramic particles, such as SiC, or to other Al particles is the oxide "skin" that is invariably present on the Al particle surface (Kim et al., 1985; Anderson and Foley, 2001). Degassing and hot pressing in an inert atmosphere contributes to the removal of Al hydrides present on the particle surface, making the oxide skin more brittle and, thus, more easily sheared (Estrada et al., 1991; Kowalski et al., 1992). The material is hot pressed, uniaxially or isostatically, to produce a fully dense composite and extruded. The rigid particles or fibers do not deform, causing the matrix to be deformed significantly.

The ratio of the reinforcement particle size to matrix particle size is very important in achieving a homogenous distribution of particles in the matrix. A comparison of the effect of Al-to-SiC particle size ratio on the composite microstructure is shown in Fig. 4.24. With the larger Al particle size, the SiC particles are "pushed" and packed in the interstices between the larger Al particles, yielding a more clustered microstructure, Fig. 4.24(a). A particle size ratio closer to one yields a more homogeneous microstructure, Fig. 4.24(b). The degree of homogeneity in particle distribution can be quantified by a clustering parameter. Several techniques have been used to quantify SiC particle clustering in metal matrix composites (Dirichlet, 1850; Lewandowski et al., 1989; Spowart et al., 2001; Yang et al., 2001). One important technique is called tesselation and is described in detail in Chapter

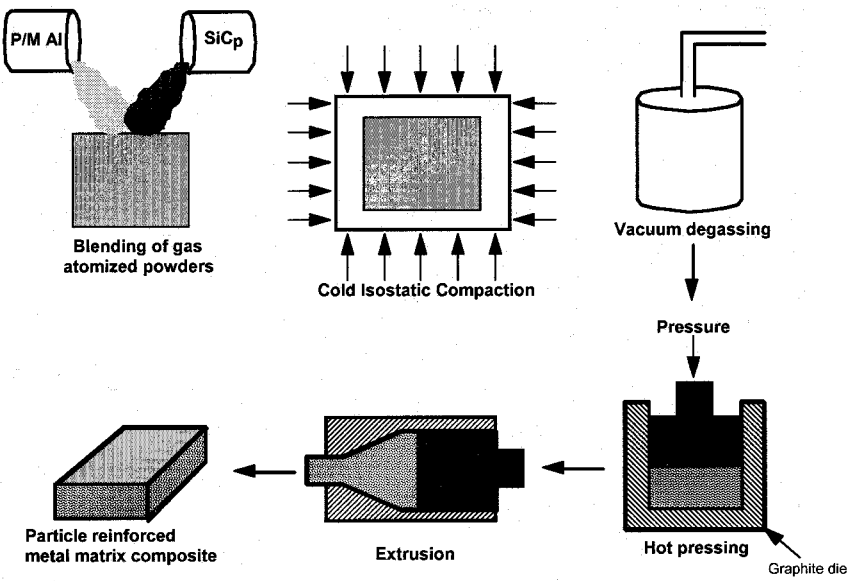


**Fig. 4.23** Powder processing, hot pressing, and extrusion process for fabricating particulate or short fiber reinforced MMCs.

7. Measurement of the nearest-neighbor distance of each SiC particle is the simplest means of assessing particle clustering but it can be deceptive, since the mean nearest neighbor spacing ignores the distribution in nearest neighbor spacings in the microstructure. Yang et al. (2001) showed that the coefficient-of-variance of the mean near-neighbor distance ($COV_d$) is particularly sensitive and effective in characterizing particle clustering. This parameter is also relatively insensitive to particle volume fraction, size, and morphology. $COV_d$ can be described by the following equation (Yang et al., 2001):

$$COV_d = \frac{\sigma_d}{d}$$

where $\sigma_d^2$ is the variance in the mean nearest-neighbor distance, and $d$ is the average of the mean near-neighbor distance of the particles sampled.

The degree of clustering, as measured by $COV_d$, as a function of Al:SiC particle size ratio is shown in Fig. 4.25. For large particle size ratios, i.e., Al particle size much greater than SiC, or vice-versa, the degree of clustering is relatively high. It is interesting to note that the minimum degree of clustering ($COV_d$) tends to a particle size ratio of about one.

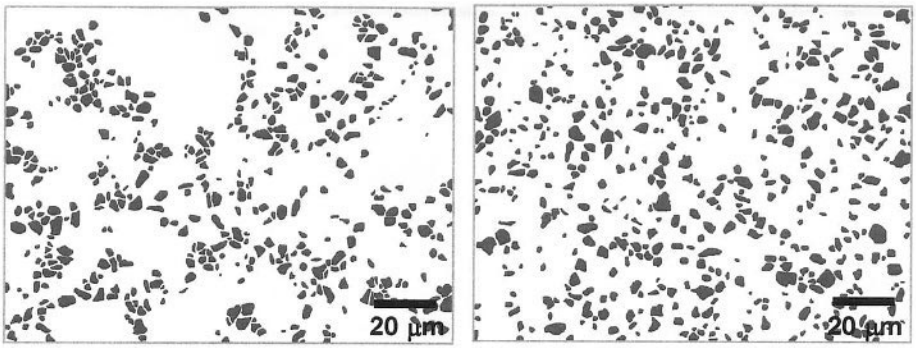


**Fig. 4.24** Particle clustering in Al/SiC/$15_p$ with different Al-SiC particle size ratios: (a) Al-SiC ratio of 6.6 ($d_{Al}$ = 33 μm, $d_{SiC}$ = 5 μm) and (b) Al-SiC ratio of 1.4 ($d_{Al}$ = 7 μm, $d_{SiC}$ = 5 μm). Increasing the Al:SiC ratio results in a greater degree of SiC clustering.

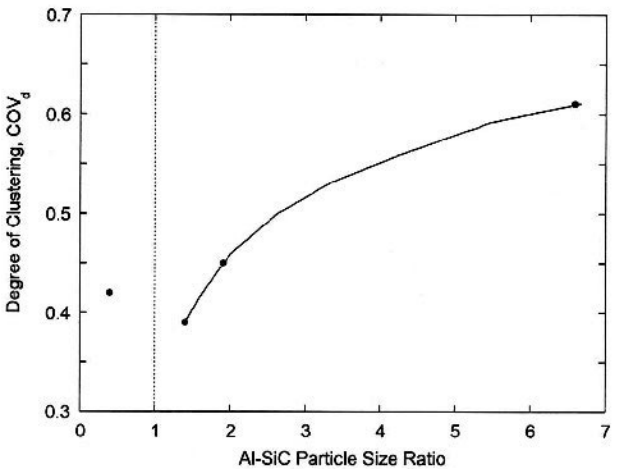


**Fig. 4.25** Degree of clustering versus Al-to-SiC particle size ratio. The degree of clustering tends to a minimum at a particle size ratio close to one.

### 4.2.2 Extrusion

Extrusion processing has been used extensively as a means of secondary deformation processing of MMCs (Ghosh, 1993; Hunt, 1994; Lloyd, 1997). It is particularly advantageous because the combination of pressure and temperature results in shear between Al/Al particles and Al/SiC particles, which contributes to fracture of the oxide skin on the Al particles, and the bonding between particle and matrix is enhanced. Because of the large strains associated with this process, however, extrusion has been used primarily to consolidate composites with discontinuous reinforcement, in order to minimize reinforcement fracture. Even in discontinuously reinforced materials, fracture of short fibers or particles often takes place, which can be detrimental to the properties of the composite.

Three types of extrusion are shown in Fig. 4.26, direct, conventional, and hydrostatic. In direct extrusion, the extruded material is deformed against a flat plate with a small orifice. This causes a "dead-metal zone" which consists of a region where the metal cannot flow. In conventional extrusion, the die is tapered to minimize the dead-metal zone. Die friction is present, however, which will result in higher deformation stresses at the metal/die interface. In MMCs, this effect is particularly exacerbated due to the presence of the particles and the large shear stresses at the metal/container interface result in material discontinuities. This can result in ragged edges, called the "christmas tree" effect, Fig. 4.27. This is more predominant with an increase in reinforcement particle content, due to the increase in die friction and, thus, shear stresses. Finally, the problems of die friction can be minimized by conducting the extrusion inside a high pressure fluid. This results in a close to hydrostatic stress state, and minimal effect of friction in the billet because the contact area between material and die is minimized.

Several microstructural changes take place during extrusion. These include alignment of particles along the extrusion axis, particle fracture (depending on the reinforcement particle size and the strains involved), and refinement and recrystallization of matrix grains (Chawla et al., 1998; Tham et al., 2002; Ganesh and Chawla, 2004; Ganesh and Chawla, 2005). Figure 4.28 shows the microstructure of SiC particle reinforced Al alloy at three different reinforcement volume fractions: 10, 20, and 30%. Note the preferred orientation of reinforcement particles along the extrusion axis.

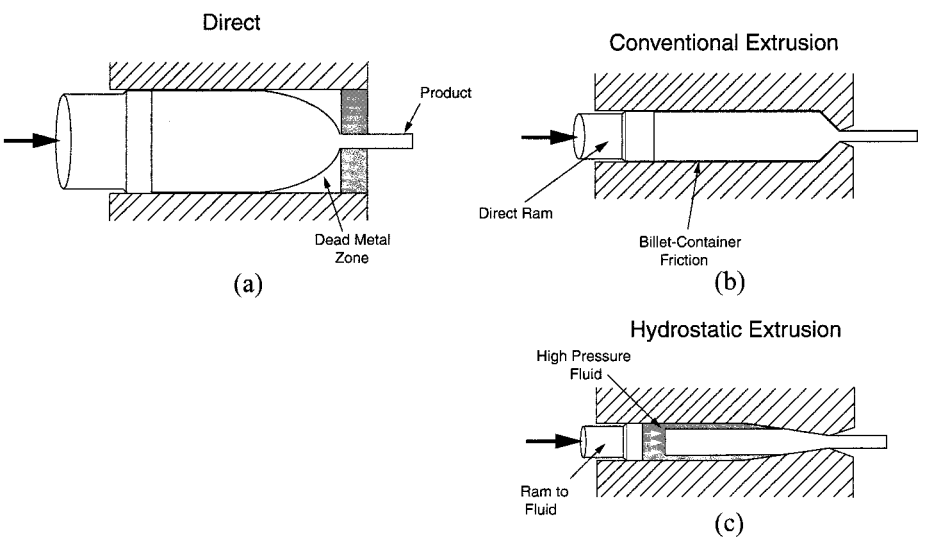


**Fig. 4.26** Three types of extrusion processing: (a) direct, (b) conventional, and (c) hydrostatic. The latter minimizes die-friction and "dead-metal" zones.

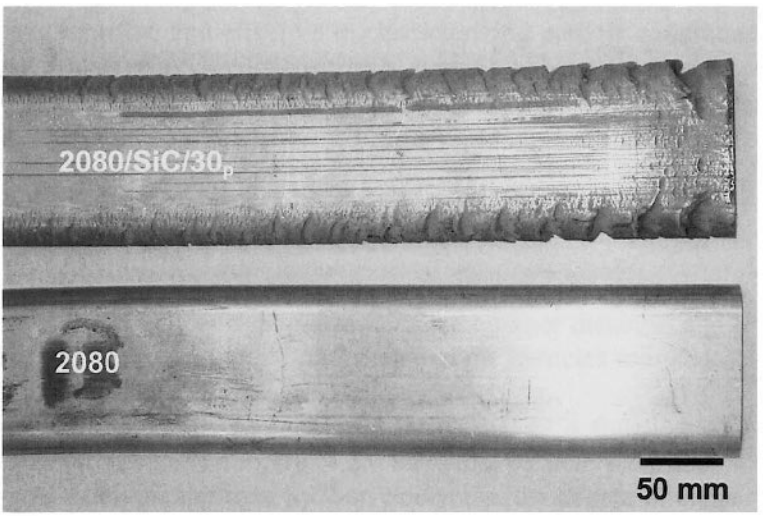


**Fig. 4.27** Comparison of extruded Al 2080 alloy and 2080/SiC/$30_p$. Note the ragged edges or "christmas tree" effect due to enhanced die friction in the composite.

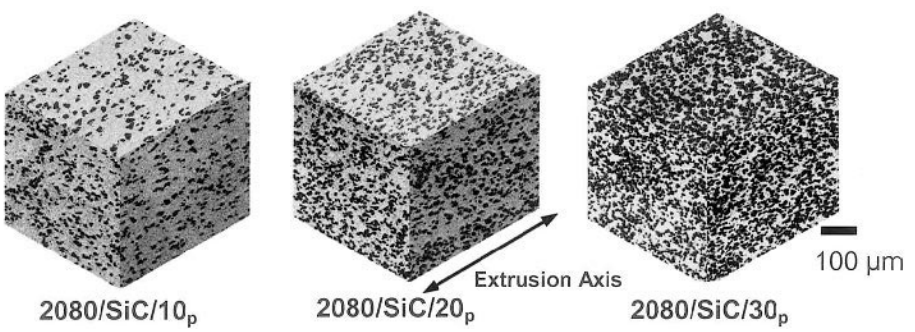


**Fig. 4.28** Microstructure of SiC particle reinforced Al alloy for three reinforcement volume fractions: 10, 20, and 30 %. Note the preferred orientation of reinforcement particles along the extrusion axis (Ganesh and Chawla, 2004).

Quantitative analysis of the degree of orientation of the particles, defined as the angle of a given particle to the longitudinal or transverse axis, shows that the degree of alignment of particles in the longitudinal plane, at a given volume fraction of particles, was much higher than that in the transverse plane, Fig. 4.29. However, the degree of orientation in the longitudinal plane decreased with an increase in volume fraction of particles. This can be explained by noting that the larger the fraction of particles, the lower the mean free path available for particle rotation and alignment along the extrusion axis. The anisotropy in particle alignment has a profound impact

on Young's modulus and tensile strength (Logsdon and Liaw, 1986; Ganesh and Chawla, 2005), and these are described in Chapter 7. Extrusion-induced particle fracture can reduce the strength of the composite significantly, often to levels below that of the unreinforced alloy (see Chapter 7).

The incorporation of reinforcement particles also has an "indirect" effect on the metal matrix grain size. As described above, with the incorporation of the hard reinforcement particles, a larger degree of plastic flow is required to deform the matrix around the particles (Chawla et al., 1998). This also results in an overall refinement in matrix grain size, shown in Fig. 4.30. The

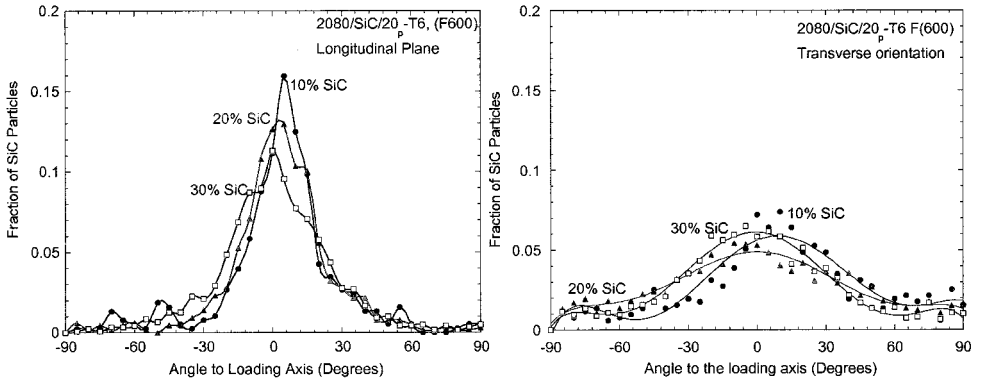


(a) (b)

**Fig. 4.29** Quantitative analysis of the degree of orientation of the particles (orientation is defined by the angle of a given particle to loading axis): (a) longitudinal and (b) transverse. The degree of alignment of particles in the longitudinal plane, at a given volume fraction of particles, is much higher than that in the transverse plane (Ganesh and Chawla, 2004).

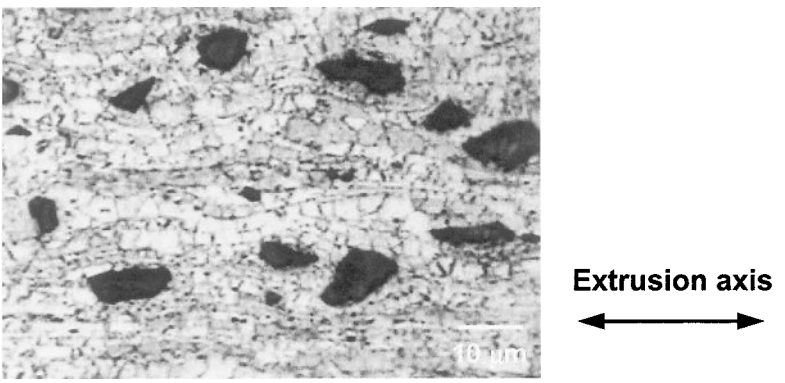


**Fig. 4.30** Microstructure of extruded 2080/SiC/$10_p$ composite (Ganesh and Chawla, 2004). The matrix grain size is refined due to the constraint on deformation from the SiC particles. Dynamic recrystallization during hot extrusion results in a finger grain structure at the particle/matrix interface.

grain size in the composite is also inhomogeneous, being smaller near the particle/matrix interface and increasing in size with increasing distance from the particle/matrix interface. The large degree of shear produced by extrusion between particles and matrix is conducive to a very strong mechanical bond between the particle and matrix. A strong mechanical bond between particle and matrix is highly desirable in strengthening of MMCs, because it maximizes the degree of load transfer from the matrix to the particle, and thus, increases the chance that a given particle will be loaded to its fracture stress (Williams et al., 2002).

During hot extrusion the particles also act as nucleating sites for recrystallization of new matrix grains, which results in a much finer grain size along the particle/matrix interface (Liu et al., 1989; Humphreys et al., 1990). This is shown in the orientation imaging map of the matrix grains in the composite, Fig. 4.31. Macroscopically, the matrix exhibits a [100]<111> texture, typical of deformation processed FCC materials. Perpendicular to the extrusion direction, the texture is random, indicating an overall fibrous texture in the material. A closer look at the grain orientation at the particle/matrix interface shows that the grains at the interface are randomly oriented, due to dynamic recrystallization, Fig. 4.32. The grains further away from the interface, however, exhibit the typical [100]<111> texture.

A disadvantage of the conventional powder metallurgy process followed by extrusion is the high cost of the process. The high cost is driven primarily by the difficulty in machining these wear-resistant composites and the material waste generated to produce a component. Thus, while the extrusion process has been used to fabricate composites for very demanding applications, particularly in the aerospace sector, it is not conducive for applications where low cost and high volume are as important as performance.

### 4.2.3 Forging

Forging is another common secondary deformation processing technique used to manufacture metal matrix composites. Once again, this technique is largely restricted to composites with discontinuous reinforcement. In conventional forging, a hot-pressed or extruded product is forged to near-net shape (Helinski et al., 1994).

A new, low cost sinter-forging technique has been developed whereby a powder mixture of the reinforcement and matrix powder is cold compacted, sintered, and forged to nearly full density, see Fig. 4.33 (Chawla et al., 2003). The main advantage of this technique is that forging is conducted to produce a near-net shape material, and machining operations and material

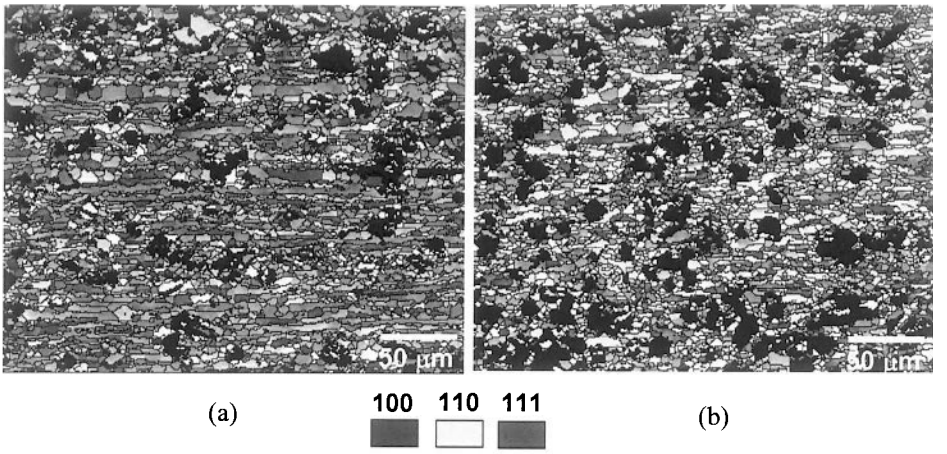


**Fig. 4.31** Orientation imaging map of matrix grains in a 2080/$SiC_p$ composite: (a) parallel to extrusion axis and (b) perpendicular to extrusion axis. The matrix exhibits a [100[<111> texture, typical of deformation processed FCC materials. Perpendicular to the extrusion direction, the texture is random, indicating an overall fibrous texture.

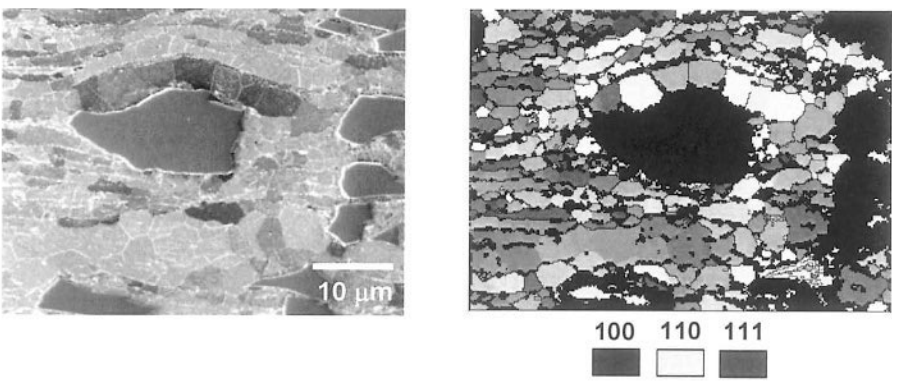


**Fig. 4.32** Grain orientation at the particle/matrix interface showing that the grains at the interface are randomly oriented, due to dynamic recrystallization.

waste are minimized. A similar process is used to manufacture ferrous connecting rods for large volume passenger car applications (James, 1985).

The microstructure of forged composites exhibits some preferential alignment of SiC particles perpendicular to the forging direction. A comparison with extruded composites, of similar particle size, indicated that the alignment in the sinter-forged composites was not as significant as that produced by extrusion (Chawla et al., 2003). This is to be expected since a much larger amount of plastic deformation is induced during extrusion. The low cost, sinter-forged composites have tensile and fatigue properties that

are comparable to those of materials produced by extrusion (Chawla et al., 2003).

The morphology of the Al grains is also affected by forging. The grains are "pancake-shaped," Fig. 4.34, with the major axis of the grains being perpendicular to the forging axis. The observed anisotropy appears to be a direct result of the constraint on lateral deformation provided by the closed die forging, so the grains are unable to deform equally in all directions.

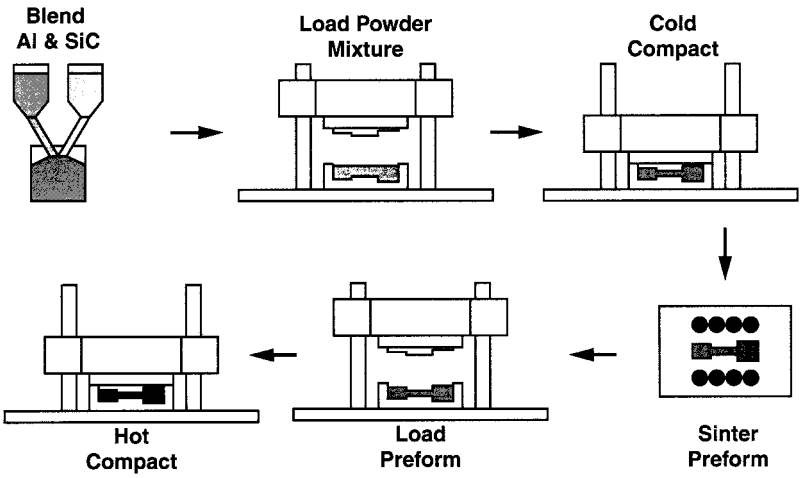


**Fig. 4.33** Schematic of near net-shape sinter-forging technique. A mixture of reinforcement powder and matrix powder is cold compacted, sintered, and forged to nearly full density (Chawla et al., 2003).

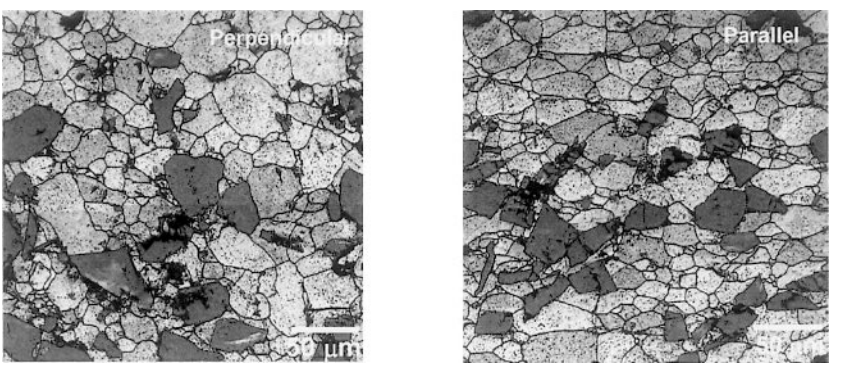


**Fig. 4.34** Morphology of Al matrix grains after forging (Chawla et al., 2003): (a) perpendicular to forging axis and (b) parallel to forging axis. The latter shows that the grains are "pancake-shaped," with the major axis of the grain being perpendicular to the forging axis.

### 4.2.4 Pressing and Sintering

A relatively inexpensive and simple technique involves pressing and sintering of powders. These composite systems are typically sintered in a temperature range to obtain some degree of liquid phase. The liquid phase flows through the pores in the compact resulting in densification of the composite (unless interfacial reaction takes place). Special mention should be made of WC/Co composites, commonly known as cemented carbides. They are really nothing but very high volume fraction of WC particles distributed in a soft cobalt matrix. These composites are used extensively in machining and rock and oil drilling operations. They are made by liquid phase sintering because liquid cobalt wets WC very well, the contact angle being 0°, with little or no interfacial reaction. Figure 4.35 shows the microstructure of such a composite, 90% WC and 10% Co. Note the angular nature of the WC particles (Deng et al., 2001).

### 4.2.5 Roll Bonding and Co-extrusion

Roll bonding is a common technique used to produce a laminated composite consisting of different metals in layered form (Chawla and Godefroid, 1984). Such composites are called sheet laminated metal-matrix composites. Roll bonding and hot pressing have also been used to make laminates of Al sheets and discontinuously reinforced MMCs (Hunt et al., 1991; Manoharan et al., 1990). Figure 4.36 shows the roll bonding process of making a laminated MMC. Figure 4.37 shows a transmission electron micrograph (TEM) of a roll-bonded Al 1100 and Al 2024 laminated composite, which exhibits the interface with very good integrity (Chawla, 1991). A larger dislocation density is observed in the Al 1100 layer, which underwent a larger

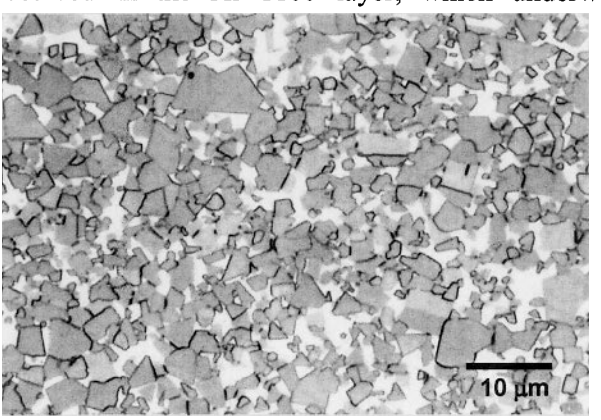


**Fig. 4.35** Microstructure of liquid phase sintered 90% WC reinforced Co matrix composite. Note the angular nature of the WC particles (Deng et al., 2001).

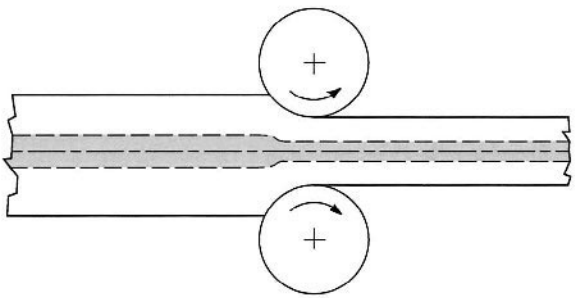

**Fig. 4.36** Roll bonding process of making a laminated MMC where a metallurgical bond is produced between the layers.

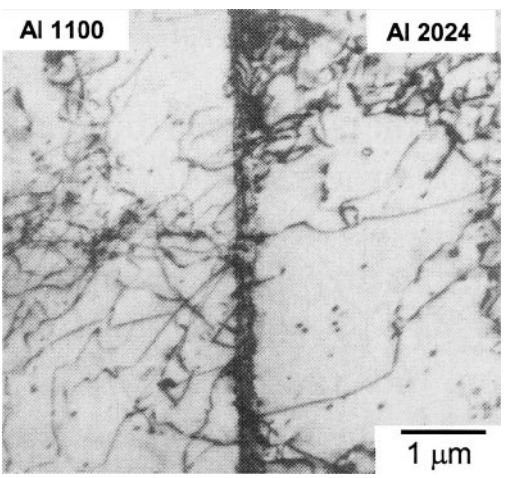


**Fig. 4.37** Transmission electron micrograph (TEM) of a roll-bonded Al 1100 and Al 2024 laminated composite, which exhibits an interface with very good integrity (Chawla, 1991). A larger dislocation density is observed in the Al 1100 layer, which is softer than Al 2024.

deformation during processing than Al 2024.

Other examples of deformation processed metal-matrix composites are niobium-based conventional filamentary superconductors with a copper matrix and high-$T_C$ superconductors with a silver matrix. There are two main types of the conventional niobium-based superconductors: Nb-Ti/Cu and $Nb_3Sn$/Cu. Niobium-titanium (~50–50) form a ductile system. Rods of Nb-Ti are inserted in holes drilled in a block of copper, evacuated, sealed, and subjected to a series of drawing operations interspersed with appropriate annealing treatments to obtain the final diameter of the composite superconductor, Fig. 4.38. In the case of $Nb_3Sn$/Cu, a process called the

bronze route is used to make this composite. $Nb_3Sn$, an A-15–type intermetallic, cannot be processed like Nb-Ti because of its extreme brittleness. Instead, the process starts with a bronze (Cu–13% Sn) matrix; pure niobium rods are inserted in holes drilled in bronze, evacuated, sealed, and subjected to wire drawing operations as in the case of Nb-Ti/Cu, Fig. 4.39. The critical step is the final heat treatment (~700°C) that drives out the tin from the bronze matrix to combine with niobium to form stoichiometric,

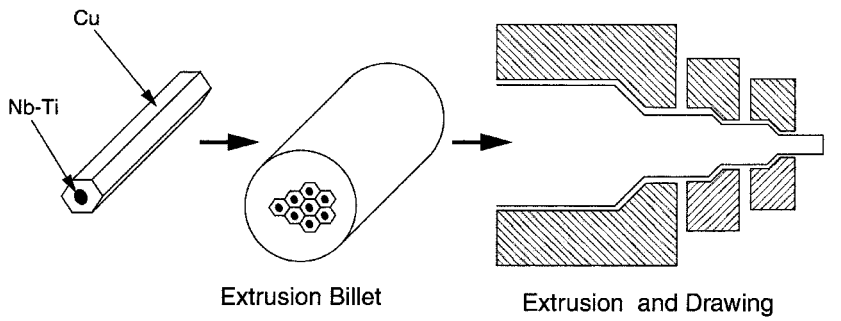


**Fig. 4.38** Extrusion-drawing route for fabricating niobium-titanium superconductors. Rods of Nb-Ti are inserted in holes in a block of copper, evacuated, sealed, and subjected to a series of drawing operations interspersed with appropriate annealing treatments to obtain the final composite superconducting wire.

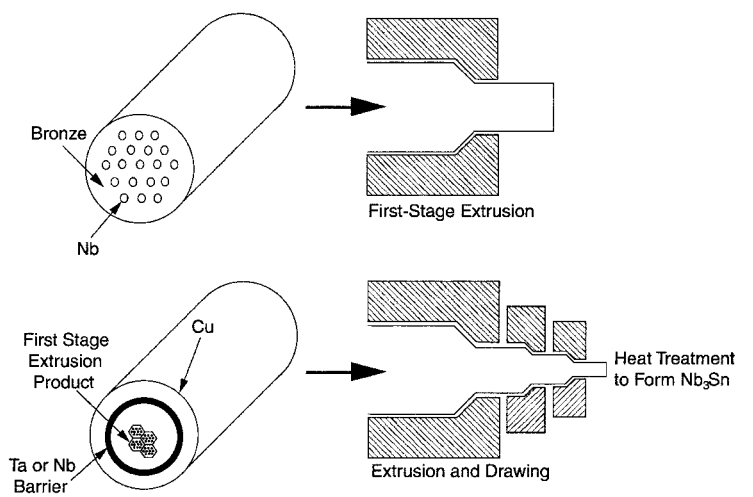


**Fig. 4.39** Process for fabricating $Nb_3Sn$/Cu superconductors. Pure niobium rods are inserted in a bronze (Cu-13% Sn) matrix, evacuated, sealed, and subjected to wire drawing operations as in the case of Nb–Ti/Cu. The critical step is the final heat treatment (~700°C) that drives out the tin from the bronze matrix to form stoichiometric, superconducting $Nb_3Sn$, leaving behind copper matrix.

superconducting $Nb_3Sn$, leaving behind copper matrix. Fig. 4.40 shows the microstructure of a $Nb_3Sn$/Cu superconductor.

In ceramic oxide (high-$T_c$) superconductors, the superconducting filaments are also brittle, so it is desirable to synthesize the brittle ceramic at the very end of this process. The metallic precursor (MP) method, involves melting the metallic elements (i.e., Y, Ca, Ba, Cu, and Ag), melt spinning the molten alloy into ribbon form, and pulverizing to obtain a homogeneous alloy powder. The precursor is packed into a silver can, sealed, and extruded into a hexagonal rod. Figure 4.41(a) shows a low magnification cross-section of a cable made by the MP process. The higher magnification view, Fig. 4.41(b), shows a transverse section of $Y_{0.9}Ca_{0.1}Ba_2Cu_4Ag_{0.65}$ (Y-124) filament/silver matrix composite containing 962,407 filaments. Another important process for ceramic superconductor metal matrix composites is the oxide-powder-in-tube (OPIT) method (Sandhage et al., 1991). In this process, the oxide powder of appropriate composition (stoichiometry, phase content, purity, etc) is packed inside a metal tube (generally silver), sealed, and degassed, Fig. 4.42. Commonly, swaging and drawing are used for making wires and rolling is used for tapes. Heat treatments, intermediate and/or subsequent to deformation, are given to form the correct phase, promote grain interconnectivity and crystallographic alignment of the oxide, and obtain proper oxygenation (Sandhage et al., 1991).

We now provide a summary of the work on so-called second generation (2G) HTS that followed the work on first generation HTS involving silver matrix containing superconducting filaments. The driving force for the 2G

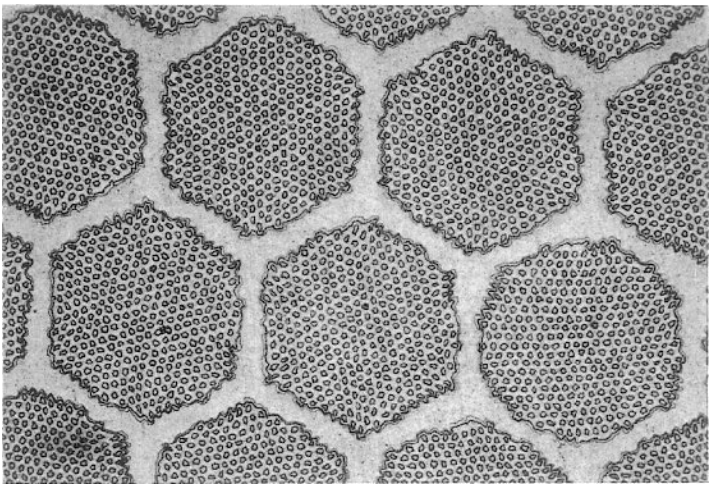

**Fig. 4.40** Microstructure of $Nb_3Sn$ filament/Cu matrix composite superconductor used in high-field magnets (courtesy of Hitachi Cable Co.).

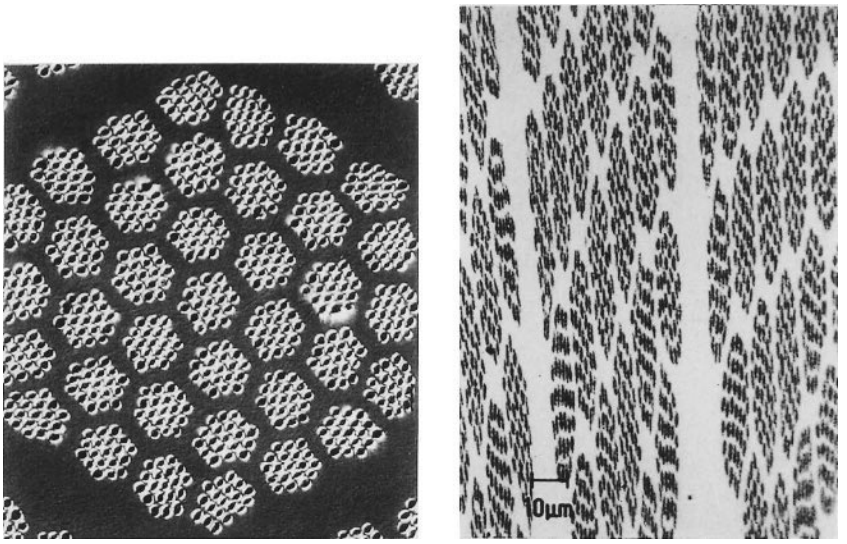


**Fig. 4.41** Microstructure of $Y_{0.9}Ca_{0.1}Ba_2Cu_4Ag_{0.65}$ (Y-124) filament/silver matrix composite cable made by melt spinning: (a) lower magnification and (b) higher magnification (courtesy of American Superconductor Co.). The cable consists of 962,407 filaments.

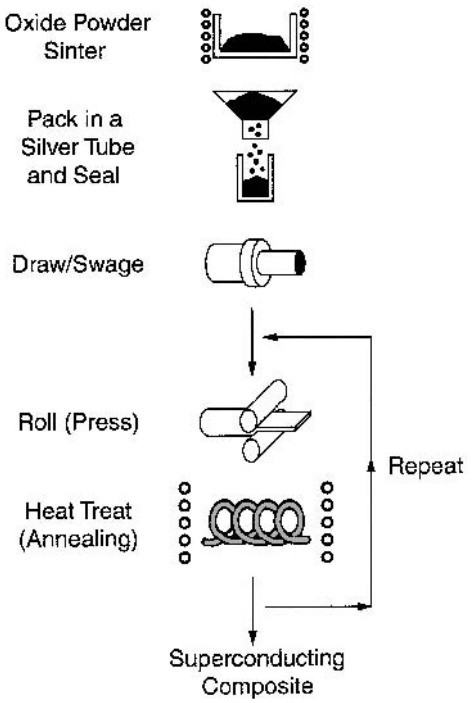


**Fig. 4.42** Oxide-powder-in-tube (OPIT) method used to fabricate silver matrix high-$T_C$ superconducting composites. The oxide powder is packed inside a metal tube (generally silver), sealed, and degassed.

work was the realization that a high temperature superconductor with randomly oriented grains will have randomly oriented grain boundaries; such misoriented grain boundaries form obstacles to the flow of superconducting current. If the grains can be aligned, i.e., produce a textured HTS, the flow of current will improve. The approach arrived at, after a considerable amount of work, consisted of epitaxial growth of YBCO on a textured template of the substrate.

The so-called second generation HTS wire consists of a long substrate in the form of a tape that has a highly textured surface. A technique developed at Oak Ridge National Laboratory, called RABiTS™ (rolling-assisted biaxial textured substrates) enables the superconducting phase to have a high degree of grain alignment (Goyal et al., 1996; Goyal et al., 1999). This textured grain structure is required for an efficient flow of current through the superconductor. The RABiTS™ process results in substrates for the HTS wire that are chemically compatible with high-temperature superconductors and exhibit sharp biaxial texture. The process is quite complex. Tape of a metal such as nickel is prepared by special rolling and heat treatment. Next, a buffer layer technology, developed specifically for these textured metals, was used to provide a chemical barrier between the nickel and the superconductor while maintaining the texture. For this, a thin layer of palladium is deposited using electron beam evaporation or sputtering. Metal oxide buffer layers, for example ceria and yttria-stabilized zirconia (YSZ), are placed on the tapes by pulsed-laser deposition. These oxide layers maintain the biaxial texture and provide a chemical barrier between the superconductor and the metal tape. This then is a RABiTS™ substrate, ready for application of the superconductor. The high-temperature superconductor yttrium-barium-copper-oxide (YBCO) is then deposited on the conditioned surface by pulsed-laser deposition. On this an epitaxial YBCO coating is deposited, which is highly textured and thus achieves the desired high superconducting current density. The term epitaxy means that the orientation of the YBCO coating matches that of the underlying substrate. Thus, the second generation (2G) high temperature superconductor (HTS) wires consists a tape-shaped substrate, on which a thin coating of $YBa_2Cu_3O_7$ (YBCO) is deposited epitaxially so that the grains of YBCO are highly aligned. This then is the basic principle for making of a second generation HTS wire: Use a long-length substrate tape with a highly textured interface and an epitaxial YBCO coating replicating the interface texture. This results in a superconductor with high current density.

### 4.2.6 Diffusion Bonding

Diffusion bonding is a common solid-state processing technique for joining similar or dissimilar metals. Interdiffusion of atoms, at an elevated temperature, from clean metal surfaces in contact with each other leads to bonding (Partridge and Ward-Close, 1993; Guo and Derby, 1995). The principal advantages of this technique are the ability to process a wide variety of matrix metals and control of fiber orientation and volume fraction. Among the disadvantages are long processing times, high processing temperatures and pressures (which makes the process expensive), and limitation on complexity of shapes that can be produced. There are many variants of the basic diffusion bonding process, although all of them involve simultaneous application of pressure and high temperature. These include:

- Foil-fiber-foil process – a matrix alloy foil or powder cloth (a mixture of matrix powder and a fugitive organic binder) and fiber arrays (composite wire) are stacked in a predetermined order, as shown in Fig. 4.43. The stacked layers are vacuum hot pressed so that diffusion bonding may take place. Hot isostatic pressing (HIP), instead of uniaxial pressing, can also be used. In HIP, gas pressure against a can consolidates the composite piece inside the can. With HIP it is relatively easy to apply high pressures at elevated temperatures with variable geometries. This process is clearly suited for flat products, although corrugated structures have also been produced.

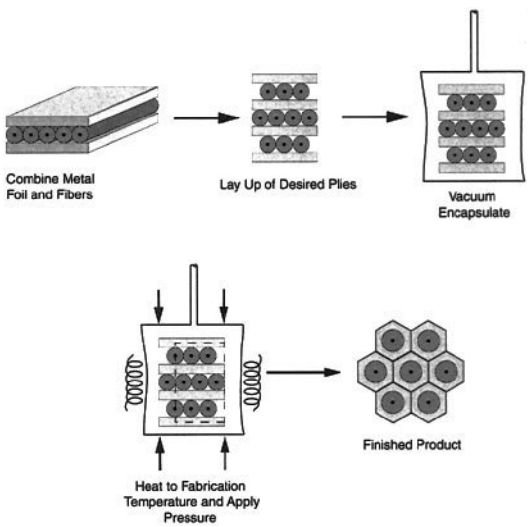


**Fig. 4.43** Foil-fiber-foil diffusion bonding process: (**a**) apply metal foil and cut to shape, (**b**) lay up desired plies, (**c**) vacuum encapsulate and heat to fabrication temperature, (**d**) apply pressure and hold for consolidation cycle, and (**e**) cool, remove, and clean part.

- Matrix coated fiber process – here the fibers are coated with the matrix material by plasma spraying or some type of physical vapor deposition (PVD) process, Fig. 4.44. The uniformity of fiber spacing is easier to control and the fibers can be handled more easily, without inducing defects deleterious to fiber strength. Depending on the flexibility of the fibers, the coated fibers may also be wound on a drum. Since the matrix volume fraction is dependent on the thickness of matrix on each fiber, very high fiber volume fraction (~80 vol.%) may be obtained. It should be noted that the fiber or fiber coatings may react or be damaged by the high impact velocity of the liquid droplets.

Fiber distribution is extremely important in controlling mechanical properties. In particular, fiber-to-fiber contact or very close spacing between fibers can result in very high, localized stress concentrations which will result in fiber cracking and/or matrix damage during processing, and premature damage, cracking and failure of the composite, under an applied load.

### 4.2.7 Explosive Shock Consolidation

A fairly novel, high strain rate, rapid solidification technique is explosive shock consolidation (Thadhani, 1988; and Thadhani et al., 1991). In this technique, dynamic compaction and/or synthesis of powders can be achieved by means of shock waves generated by either explosives in contact with the powder or high velocity impact from projectiles, Fig. 4.45. This process is particularly attractive for consolidating hard materials such as ceramics, or composites. Figure 4.46 shows an optical micrograph of a $Ti_3Al$ particle

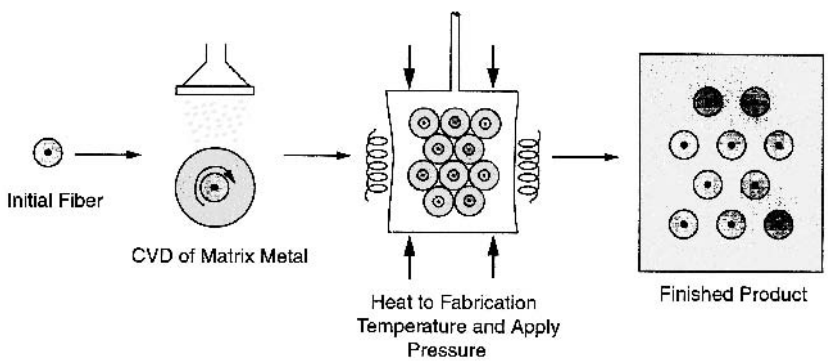


**Fig. 4.44** Matrix coated fiber process. The fibers are coated with the matrix material by plasma spraying or some type of physical vapor deposition (PVD) process.

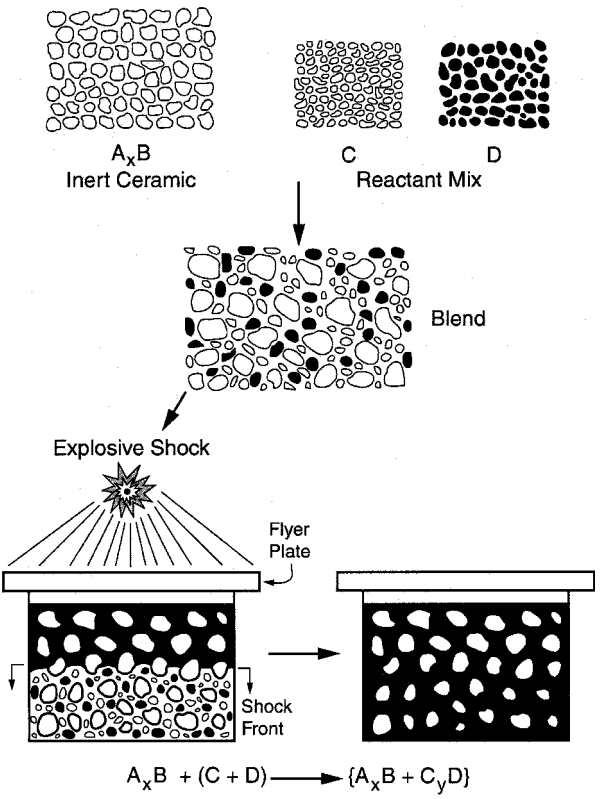


**Fig. 4.45** Dynamic compaction and/or synthesis of powders achieved by means of large shock waves generated by either explosives in contact with the powder or high velocity impact from projectiles.

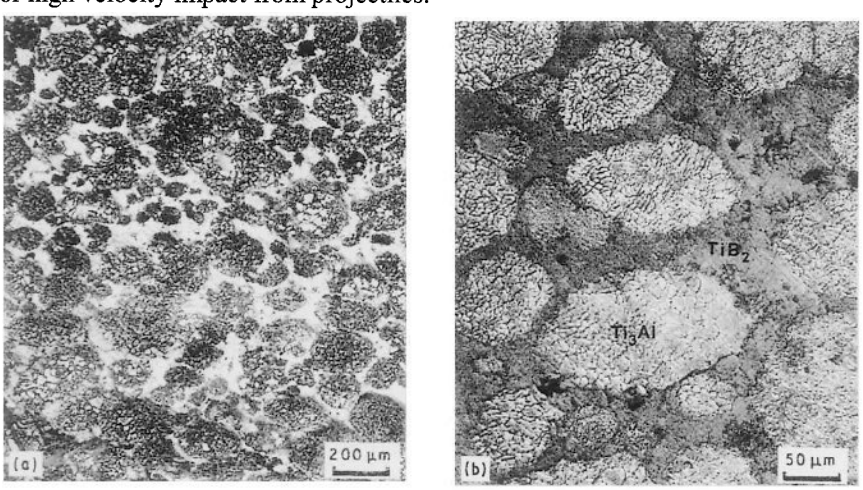


**Fig. 4.46** Optical micrographs of $Ti_3Al$ particle reinforced $TiB_2$ composite (Thadhani et al., 1991). $Ti_3Al$ particles were mixed with $TiB_2$ powder and formed a continuous matrix phase around the $Ti_3Al$ particles.

reinforced $TiB_2$ composite. In this composite, the $Ti_3Al$ particles were mixed with $TiB_2$ powder. The $TiB_2$ then formed a continuous matrix phase around the $Ti_3Al$ particles.

## 4.3 GASEOUS STATE PROCESSING

### 4.3.1 Physical Vapor Deposition

Plasma spraying is the primary form of gaseous state processing. The main application of plasma spraying was described above, to form matrix-coated fibers, which are subsequently hot-pressed to form the final product. In addition, laminated composites, particularly on the nanometer scale have been processed by PVD. PVD processes (specifically, sputter deposition-based processes) offer an extremely wide range of possibilities for fabricating nanolaminate microstructures with tailored chemistry, structure, and thickness of the individual layers and interfaces. Additional important PVD processing parameters include reactive deposition (Ji et al., 2001), plasma-assisted deposition (O'Keefe and Rigsbee, 1994), and substrate heating (Misra et al., 1998).

Some metal/metal layered systems, such as Ni/Cu and Ni/Ti, have been processed at the nanoscale by sputter deposition with great success (Misra et al., 1998; Misra and Nastasi, 1999). An example of a nanoscale Cu-Ni multilayer with a bilayer period of 5 nm is shown in Fig. 4.47 (Misra et al., 1998). Note the well-defined layered structure. The corresponding selected area diffraction pattern (inset) shows a <001> growth direction and cube-on-cube orientation relationship between FCC Cu and FCC Ni. A challenge in the synthesis of nanolaminates via the PVD approach is the control of intrinsic residual stresses. Some control over residual stresses has been achieved by energetic particle bombardment, either *in situ* or post-deposition using an ion source. In the case of magnetron sputtering, a negative substrate bias may be sufficient to change the residual stress from tensile to compressive (Misra and Nastasi, 1999). A film deposited with low bombardment energy yields a tensile residual stress and a microstructure with nanoscale columnar porosity/cracking for a sputtered 150 nm thick Cr film. The same material sputtered with a negative bias, on the other hand, yields a nanocrystalline film with an equiaxed grain structure, near-zero residual stress, and, thus, no intergranular porosity.

While metal/metal systems exhibit high strengths, metal/ceramic systems have the advantage of combining the superior properties of both ceramics and metals (Chou et al., 1992; He et al., 1998; Mearini and Hoffman, 1993;

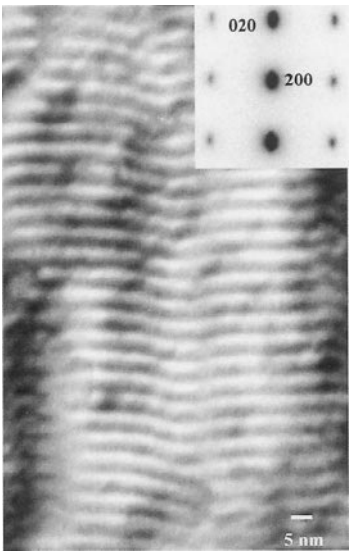


**Fig. 4.47** TEM micrograph of Cu-Ni multilayer with a bilayer period of 5 nm, by PVD (courtesy of A. Misra). Note the well-defined layered structure.

Ding et al., 1995; Deng et al., 2005). Systems such as Al/SiC and Al/$Al_2O_3$ have been investigated. Deng et al. (2005) fabricated nanolayered Al/SiC composites by RF magnetron sputter deposition. The deposition rates of Al and SiC are shown in Fig. 4.48. Note that because of the higher hardness of the SiC, removal of the SiC atoms from the substrate is more difficult, for a given beam energy, resulting in a lower deposition rate than for Al. The microstructure of an Al/SiC nanolayered composite is shown in Fig. 4.49. The sample surface was cut using a focused ion beam (FIB). The SiC layers are about 33 nm in thickness, while the Al layers are 100 nm. The layers appear to be well bonded at the interface.

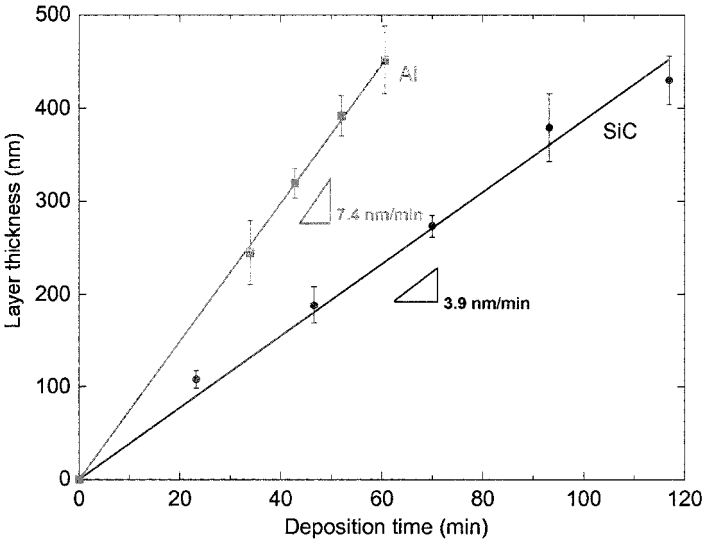


**Fig. 4.48** Layer thickness versus deposition time from physical vapor deposition (PVD) of Al and SiC (Deng et al., 2005). Since the SiC is harder, the deposition rate is lower.

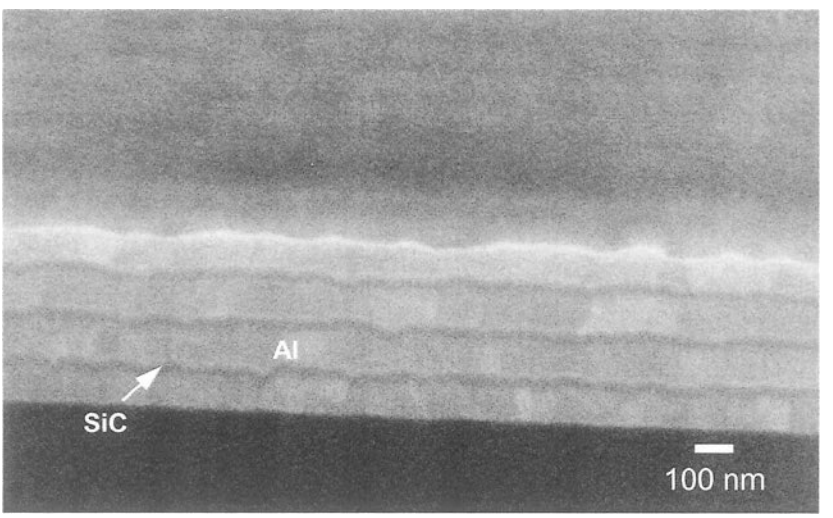


**Fig. 4.49** SEM micrograph showing the microstructure of an Al/SiC nanolayered composite, cut using a focused ion beam (FIB) (Deng et al., 2005). The SiC layers are about 33 nm in thickness, while the Al layers are 100 nm.

**References**

Aghajanian, M.K., J.T. Burke, D.R. White, and A.S. Nagelberg, (1989) *SAMPE Quarterly*, **34**, 817-823.

Anderson, I.E., and J.C. Foley, (2001) *Surf. Int. Anal.*, **31**, 599-608.

Chawla, K.K., (1991) in *Metal Matrix Composites: Mechanisms and Properties*, (R.K. Everett and R.J. Arsenault, eds.) Academic Press, New York, pp. 235-253.

Chawla, K.K., and L.B. Godefroid, (1984) *Proceedings of the 6th International Conference on Fracture,* Pergamon Press, Oxford, U.K., p. 2873.

Chawla, K.K., (1998) *Composite Materials: Science and Engineering*, Springer-Verlag.

Chawla, N., C. Andres, J.W. Jones, and J.E. Allison, (1998) *Metall. Mater. Trans.*, **29A,** 2843.

Chawla, N., J.J. Williams, and R. Saha, (2003) *J. Light Metals*, **2**, 215-227.

Chou, T.C., T.G. Nieh, T.Y. Tsui, G.M. Pharr, and W.C. Oliver, (1992) *J. Mater. Res.*, **7**, 2765-2773.

Christodolou, L., P.A. Parrish, and C.R. Crowe, (1988) *Mat. Res. Soc. Symp. Proc.*, vol. 120, 29.

Cisse, J., and G.F. Bolling, (1971) *J. Cryst. Growth*, **11**, 25-28.

Cole, G.S., and G.F. Bolling, (1965) *Trans. Metall. Soc. AIME*, **233**, 1568-1572.

Cook, A.J., and P.S. Werner, (1991) *Mater. Sci. Eng.*, **A144**, 189.

Deng, X., C. Cleveland, T. Karcher, M. Koopman, N. Chawla, and K.K. Chawla, (2005) *J. Mater. Eng. Perf.*, **14**, 1-7.

Deng, X., B.R. Patterson, K.K. Chawla, M.C. Koopman, Z. Fang, G. Lockwood, A. Griffo, (2001) *Int. J. Refrac. Metals & Hard Mater.*, **19**, 547-552.

Deve, H.E. and C. McCullough, (1995) *JOM*, **47**, 33-37.

Ding, Y., D.O. Northwood, and A.T. Alpas, (1995) *Mater. Sci. Forum*, **189**, 309-314.

Dirichlet, G.L., (1850) *J. Reine Angew. Math.*, **40**, 209-227.

Divecha, A.P., S.G. Fishman, and S.D. Karmarkar, (Sept. 1981) *J. Metals*, **9**, 12.

Estrada, J.L., J. Duszczyk, and B.M. Korevaar, (1991) *J. Mater. Sci.*, **26**, 1631-1634.

Ganesh, V.V., and N. Chawla, (2004) *Metall. Mater. Trans.*, **35A**, 53-62.

Ganesh, V.V., and N. Chawla, (2005) *Mater. Sci. Eng.*, **A391**, 342-353.

Ghosh, A.K., (1993) in *Fundamentals of Metal Matrix Composites*, Butterworth-Hinemann, Stoneham, MA, pp. 3-22.

Goyal, A., D.P. Norton, D.K. Christen, E.D. Specht, M. Paranthaman, D.M. Kroeger, J.D. Budai, Q. He, F.A. List, R. Feenstra, H.R. Kerchner, D.F.

Lee, E. Hatfield, P.M. Martin, J. Mathis, and C. Park, (1996) *Appl. Supercon.*, **4**, 403-427.

Goyal, A., R. Feenstra, F.A. List, D.P. Norton, M. Paranthaman, D.F. Lee, D.M. Kroeger, D.S. Beach, J.S. Morell, T.G. Chirayil, D.T. Verebelyi, X. Cui, E.D. Specht, D.K. Christen, and P.M. Martin, (July 1999) *JOM*, 19-23.

Guo, Z.X., and B. Derby, (1995) *Prog. Mater., Sci.*, **39**, 411-495.

He, J.L., W.Z. Li, H.D. Li, and C.H. Liu, (1998) *Surf. Coatings Tech.*, **103**, 276-280.

Helinski, E.J., J.J. Lewandowski, T.J. Rodjom, and P.T. Wang, (1994) in *World P/M Congress, vol. 7*, (C. Lall and A. Neupaver, eds.), Metal Powder Industries Federation, Princeton, NJ, pp. 119-131.

Humphreys, F.J., W.S. Miller, and M.R. Djazeb, (1990) *Mater. Sci. Tech.*, **6**, 1157-66.

Hunt, W.H., T.M. Osman, and J.J. Lewandowski, (Mar. 1991) *JOM,* 30–35.

Hunt, W.H., (1994) in *Processing and Fabrication of Advanced Materials,* The Minerals and Metal Materials Society, Warrendale, PA., pp. 663–683.

James, W.B., (1985) *Int. J. Powder Metall.*, **21**, 163.

Ji, Z., J.A. Haynes, M.K. Ferber and J.M. Rigsbee, (2001) *Surf. Coatings Tech.*, **135**, 109-117.

Katsura, M., (1982) Japan Pat. 57-25275.

Kim, J.K., and P.K. Rohatgi, (1999) *Metall. Mater. Trans.*, **29A**, 351-358.

Kim, Y.W., W.M. Griffith, and F.H. Froes, (1985) *J. Metals*, **37**, 27-33.

Kowalski, L., B.M. Korevaar, and J. Duszczyk, (1992) *J. Mater. Sci.*, **27,** 2770-2780.

Lavernia, E.J., J.D. Ayers, and T.S. Srivatsan, (1992) *Int. Mater. Rev.*, **37**, 1-44.

Lewandowski, J.J., C. Liu, and W.H. Hunt, (1989) *Mater. Sci. Eng.*, **A107**, 241-255.

Liu, Y.L., N. Hansen, and D.J. Jensen, (1989) *Metall. Trans.*, **20A**, 1743-1753.

Lloyd, D.J., (1989) *Comp. Sci. Tech.*, **35**, 159-179.

Lloyd, D.J., (1994) *Int. Mater. Rev.*, **39**, 1.

Lloyd, D.J., (1997) in *Composites Engineering Handbook* (P.K. Mallick, ed.), Marcel Dekker, New York, pp. 631-669.

Logsdon, W.A., and P.K. Liaw, (1986) *Eng. Frac. Mech.*, **24**, 737-751.

McLean, M., (1983) *Directionally Solidified Materials for High Temperature Service*, The Metals Soc., London.

Martin Marietta Corp., (1987) U.S. Patent 4,710,348.

Manoharan, M., L. Ellis, and J.J. Lewandowski, (1990) *Scripta Metall. Mater.*, **24,** 1515–1521.

Masur, L.J., A. Mortensen, J.A. Cornie, and M.C. Flemings, (1989) *Metall. Trans.* **20**, 2549-2557.

Mearini, G.T., and R.W. Hoffman, (1993) *J. Elec. Mater.*, **22** 623-629.

Mehrabian, R., R.G. Riek, and M.C. Flemings, (1974) *Metall. Trans.*, **5**, 1899-1905.

Michaud, V.C., (1993) in *Fundamentals of Metal Matrix Composites*, Butterworth-Heinneman, Stoneham, MA, pp. 3-22.

Misra, A., M. Verdier, Y.C. Lu, H. Kung, T.E. Mitchell, M. Nastasi, and J.D. Embury, (1998) *Scripta Mater.*, **39**, 555.

Misra, A., and M. Nastasi , (1999) *J. Mater. Res.*, **14**, 4466.

Mortensen, A., J.A. Cornie, and M.C. Flemings, (1988) *J. Metals*, **40**, 12.

Mortensen, A., and I. Jin, (1992) *Inter. Mater. Rev.*, **37**, 101-128.

Nourbakhsh, S., F.L. Loang, and H. Margolin, (1990) *Metall. Trans.*, **21A,** 213.

O'Keefe, M.J., and J.M. Rigsbee, (1994) *J. App. Polymer Sci.*, **53**, 1631-1638.

Partridge, P.G., and C.M. Ward-Close, (1993) *Int. Mater. Rev.*, **38**, 1-24.

Pennander, L., and C.-H. Anderson, (1991) in *Metal Matrix Composites – Processing, Microstructure and Properties*, 12th Risø Int. Symp. on Materials Science, (N. Hansen et al., eds.), Risø, Denmark, 575.

Potschke, J., and V. Rogge , *J. Cryst. Growth*, (1989) **94**, 726-738.

Saha, R., E. Morris, N. Chawla, and S.M. Pickard, (2002) *J. Mater. Sci. Lett.*, **21,** 337-339.

Sahoo, P., and M.J. Koczak, (1991) *Mater. Sci. Eng.*, **A144**, 37-44.

Sandhage, K.H., G.N. Riley, Jr., and W.L. Carter, (Mar. 1991) *JOM*, 21-25.

Shangguan, D., S. Ahuja, and D.M. Stefanescu, (1992) *Metall. Trans.*, **23A**, 669-680.

Shekhar, J.A., and R. Trivedi, (1989) *Mater. Sci. Eng.*, **A114**, 133-146.

Shekhar, J.A., and R. Trivedi (1990), in *Solidification of Metal Matrix Composites*, P. Rohatgi, ed., TMS, Warrendale, PA, pp. 23.

Spowart, J.E., B. Maruyama, and D.B. Miracle, (2001) *Mater. Sci. Eng.*, **A307**, 51-66.

Stefanescu, D.M., B.K. Dhindaw, A.S. Kakar, and A. Mitra, (1988) *Metall. Trans.*, **19A**, 2847-2855.

Surappa, M.K., and P.K. Rohatgi, (1981) *J. Mater. Sci.*, **16,** 983-993.

Thadhani, N.N., (1988) *Adv. Mater. Manuf. Proc.*, **3**, 493-549.

Thadhani, N.N., N. Chawla, and W. Kibbe, (1991) *J. Mater. Sci.*, **26**, 232-240.

Tham, L.M., M. Gupta, and L. Cheng, (2002) *Mater. Sci. Eng.*, **326**, 355-363.

Thomas, D.G., (1965) *J. Colloid. Sci.*, **20**, 267.

Trivedi, R., S.H. Han, and J.A. Shekhar, (1990) in *Solidification of Metal Matrix Composites*, P. Rohatgi, ed., TMS, Warrendale, PA, p. 23.

Tsunekawa, Y., M. Okumiya, I. Niimi, and K. Yoneyama, (1988) *J. Mater. Sci. Lett.*, **7**, 830-832.

Uhlmann, D.R., B. Chalmers, and K.A. Jackson, (1964) *J. Appl. Phys.*, **35**, 2986-2993.

Williams, J.J., G. Piotrowski, R. Saha, and N. Chawla, (2002) *Metall. Mater. Trans.*, **33A**, 3861-3869.

Yang, N., J. Boselli, and I. Sinclair, (2001) *J. Micros.*, **201**, 189-200.